Studies on Molecular Pathogenesis in Canine Epitheliotropic Cutaneous T-cell Lymphoma

（犬上皮向性皮膚 T 細胞性リンパ腫の分子病態に関する研究）

2022

The United Graduate School of Veterinary Sciences, Gifu University

(Gifu University)

KANEI, Toshitaka

CONTENTS

Chapter 3. Evaluation of pathophysiological roles of chemokine receptor 4 and 7 in a canine epitheliotropic cutaneous T-cell lymphoma model

Abbreviations

APC: Allophycocyanin

bp: Base pairs

cCCL19-hIgG-Fc: Canine CC chemokine ligand 19-human IgG-Fc fusion protein

CCK-8: Cell counting kit-8

CCL: CC chemokine ligand

CCR: CC chemokine receptor

Ct: Cycle threshold

CXCR: CXC chemokine receptor

DAB: 3,3-diaminobenzidine

DMEM: Dulbecco's modified eagle's medium

ECTCL: Epitheliotropic cutaneous T-cell lymphoma

EO-1: Canine epitheliotropic cutaneous T-cell lymphoma cell line

FBS: Fetal bovine serum

FFPE: Formalin-fixed paraffin-embedded

GAPDH: Glyceraldehyde-3-phosphate dehydrogenase

gRNA: Guide RNA

HEK: Human embryonic kidney

HPRT-1: Hypoxanthine phosphoribosyltransferase 1

IHC: Immunohistochemistry

KO: Knockout

LN: Lymph node

MF: Mycosis fungoides

NIH3T3: NIH Swiss mouse embryonic fibroblast

NOD SCID: NOD.CB17-Prkdcscid/J

p-Akt: Phosphor-Akt

PBMCs: Peripheral blood mononuclear cells

PCR: Polymerase chain reaction

RAG: Recombination-activating gene

SDS-PAGE: Sodium dodecyl sulfate-polyacrylamide gel electrophoresis

TCR-γ: T-cell receptor gamma chain

TCR: T-cell receptor

WT: Wild-type

General Introduction

Canine lymphoma is classified as multicentric, mediastinal, gastrointestinal, hepatic, renal, ocular, nervous system, and cutaneous lymphoma (84). Cutaneous lymphoma is further divided into epitheliotropic or non-epitheliotropic type based on the histopathological localization of neoplastic T-cells. Epitheliotropic type, which accounts for major cases (2), is characterized by proliferation and infiltration of neoplastic T-cells in the dermis with a specific tropism for the epidermis and adnexal structures. Dogs with epitheliotropic cutaneous T-cell lymphoma (ECTCL) show various skin lesions, including erythema, plaques, scaling, erosion, and nodules (7, 15, 16). Metastasis to the lymph nodes (LNs) and distant organs has also been observed at disease diagnosis or with disease progression (50, 53). The prognosis is generally very poor with a median survival of six months (16). Chemotherapy has been recommended treatments; however, its efficacy is frequently low. Development of novel therapies for canine ECTCL is in great demand.

According to the World Health Organization-European Organization for Research and Treatment of Cancer consensus classification, human ECTCL has more than 10 subtypes (76). Detailed information, such as incidence, prognosis, appropriate treatments, and cause of death, was described in each subtype. In contrast, canine ECTCL is classified into only three subtypes (16): mycosis fungoides (MF) (66),

pagetoid reticulosis (30), and Sézary syndrome (18). Dogs with ECTCL show various clinical presentation and course. The types and distribution of skin lesions extremely varied depending on dogs (16). Approximately 40% of dogs showed pruritus in the skin, the extent of which was also various from mild to severe. The survival duration was reported to the wide range from a few months to two years (7). Thus, there is considerable diversity in canine ECTCL, making it difficult to deal with the disease in clinical practice. In order to elucidate the differences among dogs and select an appropriate treatment for each case, further classification is necessary.

For the establishment of novel treatments and further classification, the molecular pathogenesis underlying the poor prognosis and diversity needs to be revealed. In canine ECTCL, definitive causes of death have not been elucidated; however, metastasis to LNs or distant organs may be a crucial prognostic factor because more than half of deaths from cancers are attributed to metastasis (13). Multiple skin lesions were also found to be associated with poor prognosis, which were recognized in around 90% of cases (7). Thus, systemic dissemination of neoplastic T-cells is an important phenomenon to be elucidated. A previous study investigated whether neoplastic T-cells disseminated were originated from single or multiple clone (35). Since each T-cell has an individual T-cell receptor (TCR) genes, neoplastic T-cells

generated from the same origin by clonal expansion have the identical TCR genes. The previous study evaluated the clonality of TCR genes and demonstrated that identical clones were present in different skin lesions and peripheral blood in canine ECTCL, suggesting a systemic migration of neoplastic T-cells. The finding, however, raised the question why different types of skin lesions were formed from identical neoplastic T-cells. Studies on human ECTCL showed the multiple clones of neoplastic T-cells in skin lesions from the same patients (29, 72). Further investigation on the clonality and its association with the diversity of skin lesions are required in canine ECTCL.

The migration and localization of T-cells during physiological responses are strictly controlled by the interaction between chemokines and chemokine receptors (42). Accordingly, T-cells express a regulated set of chemokine receptors that allow them to selectively respond to specific chemokines. A previous study on canine ECTCL demonstrated that chemokine receptors such as CC chemokine receptor (CCR) 4 and CCR7 were specifically translated in skin lesions (9). To elucidate the molecular pathogenesis concerning the tumor cell dynamic, therefore, the pathophysiological roles of CCR4 and CCR7 need to be investigated.

Recently, the cell line EO-1 has been established for canine ECTCL (22). Mice xenografted with EO-1 cells developed both skin lesions and systemic metastasis,

similar to dogs with ECTCL (28). These tools enabled me to conduct further investigation for clarifying the molecular pathogenesis in canine ECTCL. In this doctoral dissertation, I carried out a series of studies composed of three chapters as follows.

In chapter 1, the clonality and its association with skin lesions were investigated to reveal the identity of neoplastic T-cells and the mechanism of diversity in skin lesions.

In chapter 2, the transcription and expression of chemokine receptor CCR7 in the ECTCL cell line were examined to demonstrate the possible involvement of canine CCR7 in cancer metastasis.

In chapter 3, the effects by the knockout (KO) of CCR4 and CCR7 were evaluated in a mouse model to investigate the pathophysiological roles of chemokine receptors in canine ECTCL.

Chapter 1

Evaluation of clonality and its association with skin lesions in canine epitheliotropic cutaneous T-cell lymphoma

1.1 Introduction

Canine ECTCL is a malignant neoplasm of the skin. It is characterized by the proliferation of neoplastic T-cells with a tropism specific to the epidermis and adnexal structures (53). Approximately 90% of dogs with ECTCL exhibit multiple skin lesions, which is associated with a poor prognosis (7). The types of skin lesions markedly vary and include erythema, plaques, erosion, scaling, hypopigmentation, and nodules. Various types of skin lesions may be present at different anatomical sites in the same patients (16). Therefore, canine ECTCL is a diverse disease; however, the mechanisms underlying the formation of different skin lesions remain unclear. Chemotherapy is generally used to treat canine ECTCL, similar to other types of lymphoma (7, 52), based on the assumption that neoplastic T-cells disseminate systemically in lymphoma. Dogs with ECTCL develop not only multiple skin lesions but also metastasis to the LNs and distant organs (50, 53). Furthermore, a recent canine study indicated that all skin lesions at different anatomical sites shared identical neoplastic T-cells with the same clonalities (35). However, it currently remains unclear why different types of skin lesions are formed from identical neoplastic T-cells.

Caine ECTCL is classified into three subtypes according to the classification in

human ECTCL (15, 76). MF accounts for most cases of ECTCL in both dogs and humans. In human MF, the clonality of neoplastic T-cells has been examined at different anatomical sites. A previous study investigated the TCR gamma-chain (TCR-γ) gene rearrangement in multiple skin lesions using a polymerase chain reaction (PCR) and detected identical neoplastic T-cells in different lesions from the same patients (12). In contrast, another study using a multi-color PCR assay revealed that 39% of patients had different clones in different skin lesions (72). Furthermore, a recent study that examined the clonalities of TCR-beta by whole-exome sequencing revealed prominent clonal variations among skin lesions (29). These findings suggest that human ECTCL consists of heterogeneous neoplastic T-cells, which may be applicable to canine ECTCL. Therefore, I hypothesized that canine ECTCL also exhibits heterogeneity in the clonalities of neoplastic T-cells, which may contribute to the formation of various types of skin lesions.

In chapter 1, I conducted fragment analysis on skin lesions from dogs with ECTCL to investigate the clonality and its association with skin lesions. I employed a canine ECTCL mouse model to validate the analytical methods. I also evaluated the transcription of recombination-activating gene (RAG)1 to examine the origin of clones.

1.2. Materials and Methods

1.2.1. Samples

Twenty-five formalin-fixed paraffin-embedded (FFPE) lesional skin tissues derived from eight dogs diagnosed with ECTCL were used. Sites with noncontiguous skin lesions were selected for biopsy. The topography and types of skin lesions on biopsy sites were reviewed in medical records (Table 1-1). Peripheral blood mononuclear cells (PBMCs) were obtained from three out of eight dogs. FFPE and PBMC samples were used for DNA extraction and PCR followed by a fragment analysis. Seven skin lesions, which were preserved in RNA stabilization solution (QIAGEN), were also employed for a transcription analysis. All samples above were derived from client-owned dogs diagnosed at Animal Medical Center of Gifu University. Informed written consent on using the samples for research was obtained from all owners.

1.2.2. DNA extraction and PCR

Genomic DNA was extracted from FFPE lesional skin tissues using NucleoSpin DNA FFPE XS (Takara Bio Inc.; Shiga, Japan). The genomic DNA of each PBMC sample was also extracted using the QIAamp DNA Mini Kit (QIAGEN). Extracted genomic DNA was quantified spectrophotometrically using BioPhotometer Plus (Eppendorf; Hamburg, Germany) and adjusted to 100 ng genomic DNA per PCR reaction. Primers targeting the TCR-γ gene were prepared as previously described (21, 78): forward (5'-CGTGTACTACTGCGCTGCCTGG-3') and reverse (5'-GTGTCTTGTGCCAGGACCAAACACTT-3'). The forward primer was labeled with fluorescent dye at its 5′ end. PCR reactions were performed using Amplitaq Gold 360 Master Mix (Thermo Fisher Scientific; Waltham, MA, USA) on Takara Thermal Cycler Dice (Takara Bio Inc.). Cycle conditions consisted of an initial denaturation and enzyme activation step at 95°C for 5 min, followed by 40 cycles of denaturation at 94°C for 15 sec, annealing at 62°C for 30 sec, extension at 72°C for 30 sec, and final extension at 72°C for 30 min (21). All samples were examined in duplicate.

1.2.3. Fragment analysis

One microliter of a 50-fold diluted PCR product mixture was mixed with 8.5

μL of Hi-Di formamide (Thermo Fisher Scientific) and 0.5 μL of 600 LIZ size standard v2.0 (Thermo Fisher Scientific). PCR products were denatured and size-separated using the ABI 3500 Genetic Analyzer (Thermo Fisher Scientific) with a G5 filter. The data obtained were visualized as fluorescence peaks in the form of a histogram by GeneMapper Software 6 (Thermo Fisher Scientific). A neoplastic clonal pattern was identified only if the height of one or more prominent peaks within the valid range were greater than twice the polyclonal/background signal, and the same peaks were recognized in duplicate runs. A clonal pattern was considered identical within a case when the difference in each peak size was less than 1 base pair (bp).

1.2.4. Validation of analytical methods

To validate analytical methods, an ECTCL mouse model was prepared using EO-1 cells according to the methods previously described (28). NOD.CB17-Prkdcscid/J (NOD SCID) mice were purchased from Charles River Laboratories Japan, Inc. (Yokohama, Japan). EO-1 cells were developed in my laboratory (22). Primary skin and metastatic lesional tissues, such as the spleen, lung, and blood cells, were collected from four mice and converted to FFPE samples. DNA extraction, PCR, and the fragment

analysis were conducted as described above in each sample.

1.2.5. Evaluation of histopathological features

The presence or absence of the epidermal and dermal features of ECTCL (Figure 1-1), such as lymphocytic aggregation, Pautrier's microabscess, obliteration, spongiosis, acanthosis, apoptosis, edema, and lymphocytic infiltration into adnexal structures, was evaluated (Table 1-2)(16). The coincidence rates of these histopathological features were calculated in a pair of skin lesions in each case. The presence or absence of several features was not examined in some erosive lesions due to epidermal obliteration.

1.2.6. Transcription analysis of rag1

Total RNA was extracted from seven skin lesions using the RNeasy Lipid Tissue Kit (QIAGEN). Total RNA was also extracted from the thymus and LN of a healthy female beagle dog as positive and negative controls, respectively, for RAG1. The reverse transcription of total RNA was performed to generate single-strand cDNA

for use as a template in PCR with the PrimeScript™ RT Reagent Kit (Takara Bio Inc.). PCR primers were designed based on the predicted sequences of canine *rag1* (GenBank accession number, XM_038423502.1): forward (5'-GCGGTCTCTTGAAAAGGCAC-3') and reverse (5'-CTTGGGTTTTGCCATCCACG-3'). PCR primers for glyceraldehyde-3-phosphate dehydrogenase (GAPDH) were also prepared as previously described (48). Template cDNA was amplified by PCR using PrimeSTAR Max DNA Polymerase (Takara Bio Inc.). PCR amplification was performed by 35 cycles of denaturation (98°C, 10 sec), annealing (58°C, 10 sec), and polymerization (72°C, 30 sec) (21). PCR products were electrophoresed on a 2% agarose gel containing the DNA fluorescence staining reagent Midori Green Advance (NIPPON Genetics; Tokyo, Japan). Gels were examined with ImageQuant LAS 500 (GE Healthcare UK Ltd., Buckinghamshire, England). All procedures regarding a beagle dog and mice in chapter 1 were approved by the Institutional Animal Care and Use and Clinical Ethics Committees of Gifu University (Accession number: 15001, 2020-254).

1.2.7. Statistical analysis

In a pair of skin lesions in each case, the types of skin lesions were classified as

the same or different and were compared among the clonal patterns (Table 1-3). Fisher's exact test was used to evaluate the relationship between clonal patterns and types of skin lesions. The Wilcoxon–Mann–Whitney test was used to compare the coincidence rates of histopathological features between clonal patterns. A value of $P < 0.05$ was considered significant. Statistical analyses were performed using the JMP 16.2.0 program (SAS Institute; Gary, NC, USA).

1.3. Results

1.3.1. Clonal patterns

The results of the clonal patterns in skin lesions and PBMCs are summarized in Table 1-1. The fragment analysis revealed that only case 7 had an identical clonal pattern in all three skin lesions, which was also identical to that in PBMCs (Figure 1-2 a). Four of the seven other cases exhibited identical and non-identical clonal patterns between skin lesions (Figure 1-2 b). In three cases, all clonal patterns were non-identical (Figure 1-2 c).

1.3.2. Validation of analytical methods

In ECTCL mouse models, clonal patterns were identical in all primary skin and metastatic lesions, such as spleen, lung, and blood cells (Figure 1-3).

1.3.3. Association of clonal patterns with skin lesions

Fisher's exact test showed that clonal patterns were not associated with the types of skin lesions (P = 1.000) (Table 1-3). The coincidence rates of histopathological features between skin lesions were 80.2 ± 15.5 and 67.8 ± 18.0% for identical and non-identical clonal patterns, respectively (Table 1-4). The Wilcoxon–Mann–Whitney test showed no significant difference in coincidence rates between identical and non-identical clonal patterns (P = 0.0907).

1.3.4. Transcription of rag1 in skin lesions

The transcription analysis did not detect *rag1* mRNA in any ECTCL skin lesions (Figure 1-4).

1.4. Discussion

In chapter 1, the fragment analysis identified different neoplastic clones among skin lesions from dogs with ECTCL. A previous canine study demonstrated that all skin lesions shared identical clones (35), which contradicts my results. Since canine TCR-γ genes consist of multiple sets of V and J gene segments (37), multiplex PCR was conducted using 6 forward primers and 7 reverse primers to cover various parts of TCR genes in the previous study (35). Multiplex PCR is useful for detecting clonality for a diagnosis of ECTCL (36), whereas numerous peaks amplified with multiplex PCR are not frequently reproducible, which may lead to the misinterpretation of results in a fragment analysis. In the previous study, some peaks were not reproducible between skin lesions, which were excluded from the analysis when comparing clonal patterns. On the other hand, all peaks were reproducible and comparable between skin lesions due to the small number of conspicuous peaks amplified by single primer pair in the results of chapter 1. My fragment analysis was validated using ECTCL cell line xenograft mouse models; however, further studies are needed to establish whether multiplex PCR or PCR with a single primer pair is more beneficial when investigating the identity of neoplastic clones. The primer set used in this study was designed to

recognize the wide ranges of TCR-γ genes in previous studies (21, 78). No amplification in PCR was not observed in my results; however, further studies are also necessary to evaluate the sensitivity of this primer set.

The findings of clonal heterogeneity prompted me to examine the association of clonal patterns with the types of skin lesions and histopathological features, assuming that skin lesions with an identical clone were similar to each other. However, this study revealed no significant difference between identical and non-identical clonal patterns. In human ECTCL, various skin lesions were observed in identical cases, similar to canine ECTCL (16, 38). Accumulated evidence also indicates that the types of skin lesions are dynamically altered from erythema to plaques, erosion, and nodules with disease progression (38, 76). Therefore, variations in skin lesions in canine ECTCL may be attributed to differences in progression in individual lesions rather than the clonal heterogeneity of neoplastic T-cells.

To recognize various antigens, the diversity of TCR repertoires is generated by the rearrangement of the TCR V, D and J gene segments with RAG (65). Therefore, RAG is expressed in developing T cells in the thymus, but not in proliferating cells in peripheral blood and tissues. A number of studies have investigated the expression of RAG in tumor cells. Human T-cell leukemia cell lines, such as Willow89, MOLT14,

DND41, and HPB-ALL, were shown to express RAG1 (81). In clinical cases, RAG expression was found in human T-cell leukemia and T-cell lymphoma (40). Thus, the expression of RAG was also shown in peripheral neoplastic T-cells not only in developing T-cells in the thymus. Therefore, I hypothesized that different TCR clones may be generated in individual skin lesions, which may be demonstrated by RAG expression. However, *rag1* was not translated in any skin lesions, indicating that different clones originated not in the skin, but elsewhere. In a recent human study, multiple TCR clones were detected in peripheral blood (29). In a previous canine study, in addition to an identical clone in skin lesions, another unique clone was also detected in peripheral blood (35). Collectively, my results and previous findings identified that neoplastic clonal heterogeneity in canine ECTCL may develop in peripheral blood rather than in the skin. Further studies are needed to investigate clonality in peripheral blood and the origin of clonal heterogeneity.

The results also demonstrated that identical clones were present in different anatomical sites, indicating that neoplastic T-cells migrated systemically in canine ECTCL. Since the systemic dissemination of neoplastic T-cells was a crucial phenomenon contributing to poor prognosis (7), the mechanism of tumor cell migration needs to be elucidated. The migration and localization of lymphocytes during

physiological responses are strictly controlled by the interaction between chemokines and chemokine receptor (42); therefore, further studies focusing on chemokines are needed.

In conclusion, I demonstrated that clonal heterogeneity of cutaneous neoplastic T-cells in canine ECTCL, which was not associated with the clinical or histopathological features of skin lesions. The results of chapter 1 suggest that different clones originated not in the skin, but elsewhere, such as peripheral blood. The migration of neoplastic T-cells was also indicated, which requires further investigation on the involvement of chemokines

1.5. Table and Figure

Case	Breed	Age (years)	Sex	DNA		Skin mRNA No.	Skin lesion		Clonal pattern	
				PBMCs	Skin		Topography	Type	Skin	PBMCs
1	Maltese	17	F		1-a	1	Dorsum	Erythema	1-1	
					1-b	2	Abdmen	Erythema	1-2	
					1-c		Dorsum	Plaque	1-2	
					1-d		Abdmen	Erosion	1-3	
2	Miniature dachshund	5	F	+	2-a	3	Abdmen	Plaque	2-1	P
					2-b	4	Abdmen	Plaque	2-2	
3	Airedale terrier	12	SF	+	3-a	5	Thorax	Erosion	3-1	
					3-b	6	Thorax	Erosion	3-2	P
					3-c		Abdmen	Erythema	3-3	
4	Miniature dachshund	14	M		4-a		Nose	Depigmentation	4-1	
					4-b		Lip	Erythema	4-2	
					4-c		Lip	Nodule	4-2	
					4-d		Abdmen	Erythema	4-2	
5	Papillon	10	CM		5-a		Thorax	Erosion	5-1	
					5-b		Thorax	Erosion	5-2	
					5-c		Thigh	Erosion	5-2	
6	Toy poodle	8	F		6-a		Lip	Erosion	6-1	
					6-b		Lip	Erosion	6-2	
					6-c		Lip	Erosion	6-3	
7	Yorkshire terrie	13	CM	+	7-a	7	Thorax	Erythema	7-1	
					7-b		Thorax	Erythema	7-1	7-1
					7-c		Abdmen	Erythema	7-1	
8	English bulldog	6	F		8-a		Thorax	Plaque	8-1	
					8-b		Dorsum	Plaque	8-2	
					8-c		Perineum	Nodule	8-2	

M, Male; CM, Castrated male; F, Female; SF, Spayed female
+, PBMCs were preserved.
P, Polyclonal

Table 1-1. Summary of sample information and clonal patterns.

The information of dogs and samples was shown. The results of clonal patterns were demonstrated as number or polyclonal. The same numbers of clonal patterns represent identical.

Sample	Epidermis						Dermis		
	Lymphocytic aggregation	Pautrier's microabcessation	Obliteration	Apoptosis	Acanthosis	Spongiosis	Lymphocytic aggregation	Lymphocytic infiltration into adnexal structures	Edema
1-a	+	−	−	−	−	−	+	+	+
1-b	−	−	−	−	−	−	+	+	+
1-c	+	+	−	−	−	−	+	+	+
1-d	−	−	−	−	+	−	+	+	−
2-a	+	−	−	−	+	+	+	+	+
2-b	+	+	−	+	+	+	+	−	+
3-a	+	+	−	+	+	−	+	+	+
3-b	+	−	−	−	+	−	−	+	+
3-c	−	−	−	−	+	+	+	+	+
4-a	+	−	−	−	+	−	−	−	+
4-b	+	−	−	−	+	−	−	−	−
4-c	−	−	−	−	+	−	+	+	−
4-d	+	−	−	−	+	−	+	+	+
5-a	+	+	+	+	+	−	+	+	+
5-b	+	ND	+	ND	ND	ND	+	+	+
5-c	+	+	+	+	+	−	+	+	+
6-a	ND	ND	+	+	ND	ND	+	ND	ND
6-b	ND	ND	+	+	+	ND	+	ND	+
6-c	ND	ND	+	+	+	ND	+	ND	+
7-a	+	−	−	−	−	−	+	+	+
7-b	+	−	−	−	−	−	+	+	+
7-c	+	−	−	−	−	−	+	+	+
8-a	−	−	−	−	−	−	+	+	+
8-b	−	−	−	−	+	−	+	+	+
8-c	+	−	+	−	+	−	+	+	+

+, Presence; −, Absence; ND, Not determined

Table 1-2. Evaluation of histopathological features in each skin lesion.

Presence or absence of nine histopathological features were evaluated.

		Type of skin lesion		
		Same	Different	Total
Clonal pattern	Identical	5	4	9
	Non-identical	9	10	19
	Total	14	14	28

Table 1-3. Association between clonal patterns and types of skin lesions.

In a pair of skin lesions in each case, clonal patterns were divided into identical or non-identical. The types of skin lesions were classified as the same or different and were compared among the clonal patterns. Fisher's exact test showed clonal patterns were not associated with the types of skin lesions ($P = 1.000$)

Case	Pair of skin lesions	Clonal pattern	Coincidence rate (%)
1	a-b	NI	88.9
	a-c	NI	88.9
	a-d	NI	66.7
	b-c	I	77.8
	b-d	NI	77.8
	c-d	NI	55.6
2	a-b	NI	66.7
3	a-b	NI	66.7
	a-c	NI	55.6
	b-c	NI	66.7
4	a-b	NI	88.9
	a-c	NI	55.6
	a-d	NI	77.8
	b-c	I	66.7
	b-d	I	66.7
	c-d	I	77.8
5	a-b	NI	55.6
	a-c	NI	100.0
	b-c	I	55.6
6	a-b	NI	33.3
	a-c	NI	33.3
	b-c	NI	55.6
7	a-b	I	100.0
	a-c	I	100.0
	b-c	I	100.0
8	a-b	NI	88.9
	a-c	NI	66.7
	b-c	I	77.8

I, Identical; NI, Non-identical

Table 1-4. Clonal patterns and coincidence rates in histopathology between skin lesions. The averages of coincidence rates in histopathological features were shown in pair of skin lesions with identical or non-identical clonal patterns. The Wilcoxon–Mann–Whitney test showed no significant difference in coincidence rates between identical and non-identical clonal patterns ($P = 0.0907$).

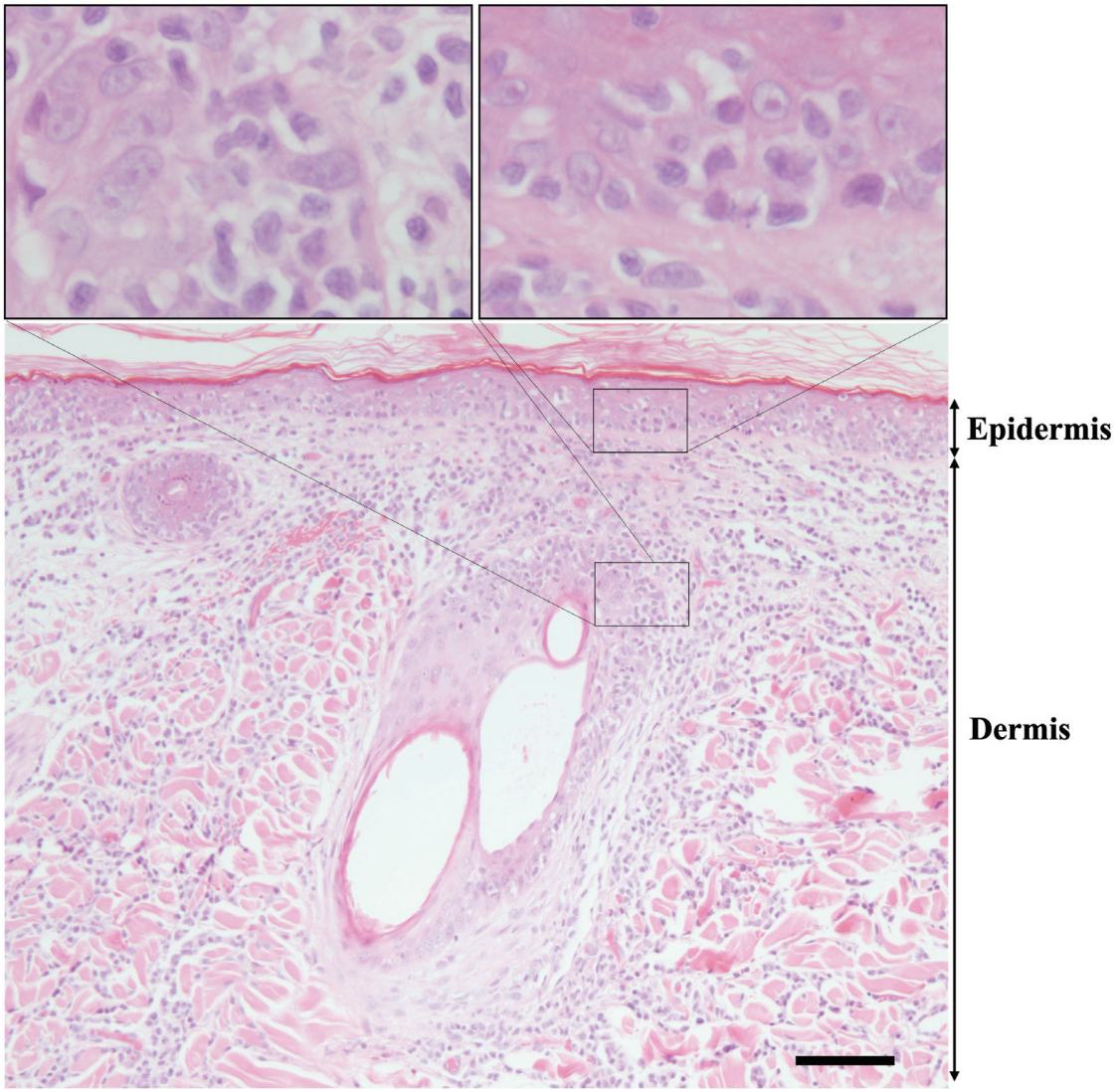

Figure 1-1. A representative image of skin lesions from dogs with ECTCL. Histopathological slides were five-micrometer thick stained with hematoxylin and eosin. Neoplastic T-cells were shown to infiltrate into the epidermis and adnexal structure. Scale bar: 100 μm.

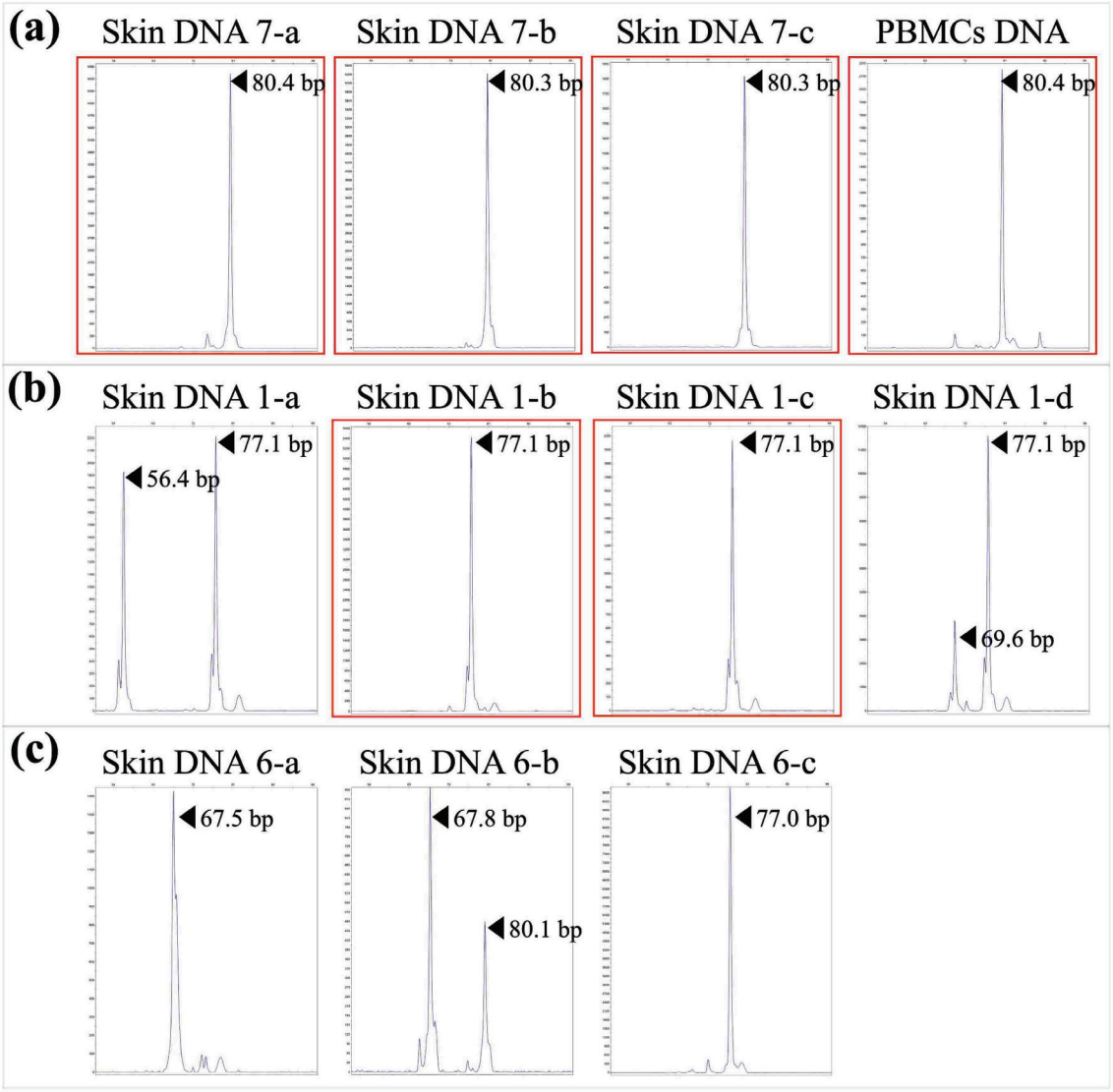

Figure 1-2. Representative clonal patterns from three cases.

Histograms were highlighted in red when clonal patterns were identical. (a) Case 7: All skin lesions and PBMCs had an identical clonal pattern. (b) Case 1: Identical and non-identical clonal patterns were both observed between skin lesions. (c) Case 6: Clonal patterns in skin lesions were all non-identical.

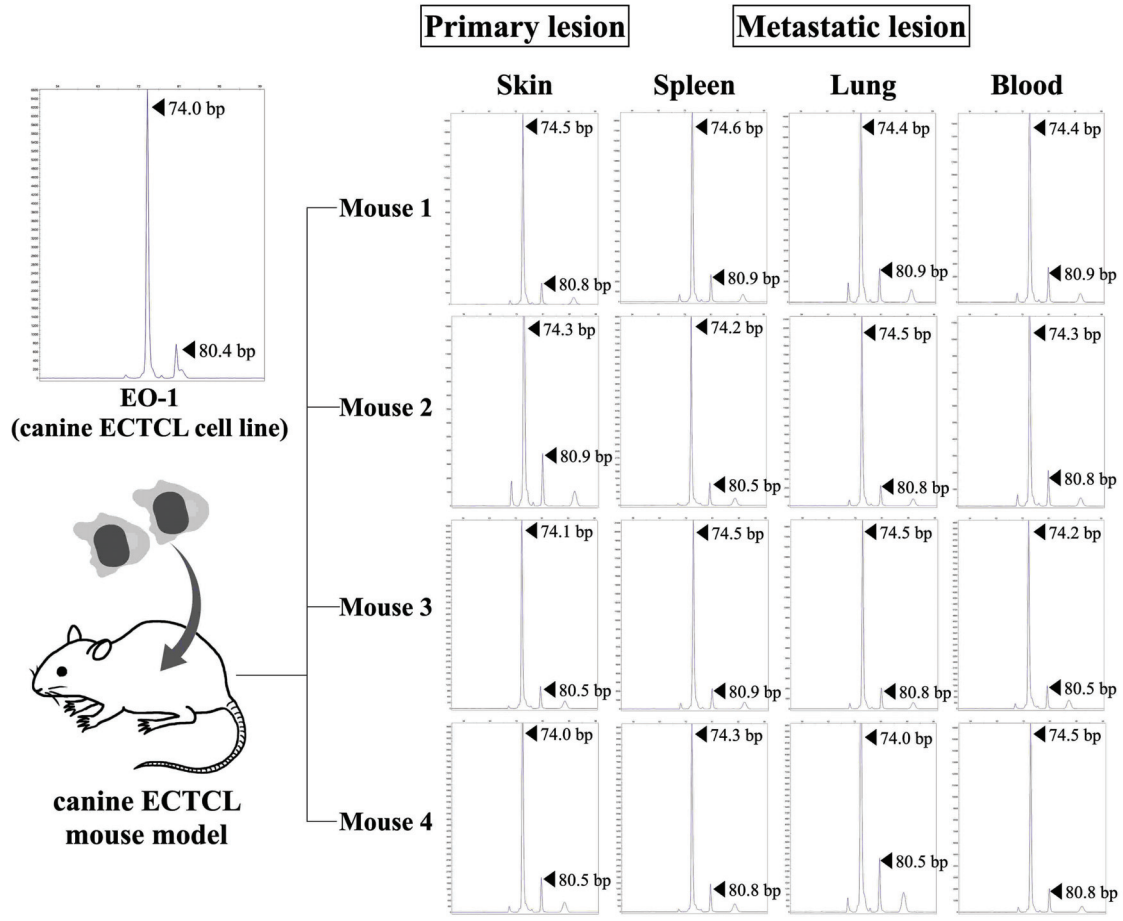

Figure 1-3. Validation for analyzing a clonal pattern in canine ECTCL mouse models. Four NOD SCID mice were subcutaneously xenografted with EO-1 cells, which showed a clonal pattern with distinct peaks at 74 and 80 bp. An identical clonal pattern was recognized in all primary skin and metastatic lesions, such as spleen, lung, and blood cells of mice.

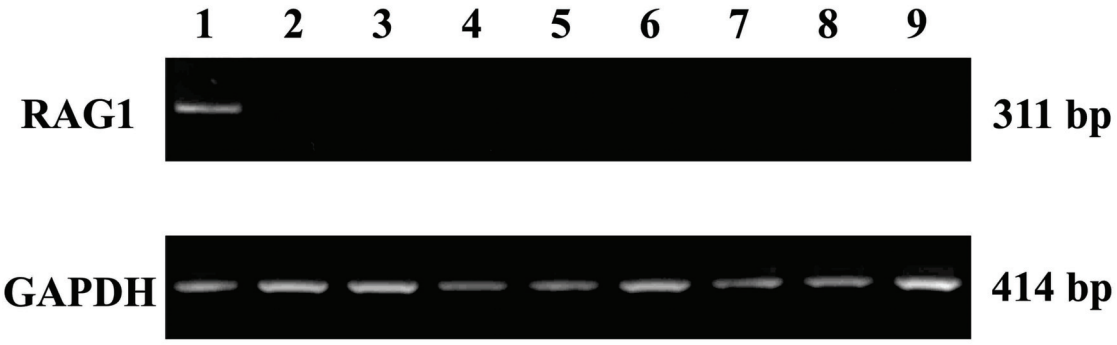

Figure 1-4. Transcription analysis of RAG1.

Canine RAG1 mRNA (upper lane) and GAPDH mRNA (lower lane) were detected by RT-PCR using specific primers to canine RAG1 and GAPDH cDNAs. Lane 1: normal canine thymus (positive control), Lane 2: normal canine LN (negative control), Lane 3-9: skin mRNA No.1-7.

Chapter 2

Expression and functional analysis of chemokine receptor 7 in a canine epitheliotropic cutaneous T-cell lymphoma cell line

2.1. Introduction

Chemokines are a large family of chemotactic cytokines that induce the directional cell migration called chemotaxis. Structurally, chemokines are classified into four families; CC, CXC, C, and CX3C, on the basis of the number and location of two of four conserved cysteine residues (86). Each chemokine has corresponding chemokine receptors, contributing to the specificity of chemotaxis. Lymphocytes that express chemokine receptors follow a signal of increasing chemokine concentration towards the source of the chemokine (4). Thus, the migration and localization of lymphocytes during physiological immune responses are strictly controlled by the interaction between chemokines and chemokine receptors (42, 46).

A previous study on canine ECTCL showed that the transcription levels of CCR4 and CCR7 were significantly higher in skin lesions than in normal skin (9). In canine ECTCL cell line, CCR4 was also highly translated compared to other canine T-cell lymphoma cell lines (22). Furthermore, the ECTCL cell line has shown to express functional CCR4 which exhibits the active chemotaxis to both the canine and murine ligand. However, the expression and function of CCR7 have not been investigated.

CCR7 and its CC chemokine ligands (CCL) 19 and CCL21 are known to play

important roles in the functions of cell homing to LNs. CCL19 and CCL21 are abundantly distributed in LNs, high endothelial venules, and afferent lymphatic vessels in which T-cells and dendritic cells accumulate (5, 17, 64). Therefore, the CCR7, CCL19, and CCL21 axis forms organized cellular microcompartments in LNs and contributes to the homeostasis of the immune system. Recent human studies reported that CCR7 is expressed not only in immune cells, but also in various tumors including lymphoma (79), and breast (55), gastric (49), and lung cancers (67). Furthermore, the expression of CCR7 in some tumors has been correlated with LN metastasis (60). In a mouse model, the knockdown of CCR7 in a colorectal cancer cell line decreased LN metastasis (83). In comparisons with control cells, murine melanoma cells transfected to express CCR7 were found to enhance LN metastasis (68). The findings of these human and mouse studies implicate CCR7 in LN metastasis in cancer patients.

In canine ECTCL, dogs have shown metastasis to LNs and distant organs (7, 50, 53). In chapter 1, I demonstrated that neoplastic T-cells disseminated at different anatomical sites showed the identical clonalities, indicating a systemic migration of neoplastic T-cells. My results and previous findings from transcription analysis (9) suggest that CCR7 may be related to the migration of neoplastic T-cells into LNs in canine ECTCL; however, the involvement of CCR7 in LN metastasis remains unknown

in canine cancers. Previous canine studies employed anti-human CCR7 antibodies (25, 80); however, their cross-reactivity and specificity to canine CCR7 were not validated. To date, there are no antibodies whose specificity to canine CCR7 has been proven. To detect canine CCR7, the use of a fusion protein combining human CCL19 with human IgG has been reported as an alternative method (24). However, it is unclear whether the fusion protein binds to canine CCR7 because its specificity was not confirmed.

In chapter 2, I evaluated the specificity of the canine CCL19 fusion protein combined with human IgG-Fc by validation with canine CCR7-transfectants. Thereafter, I analyzed the expression and function of CCR7 in the canine ECTCL cell line by comparing to other canine T-cell lymphoma cell lines to investigate the involvement of CCR7 in LN metastasis of canine ECTCL.

2.2. Materials and Methods

2.2.1. Canine CCL19-human IgG-Fc fusion protein

Canine CCL19-human IgG-Fc fusion protein (cCCL19-hIgG-Fc) was prepared as previously described (11, 23). Concisely, canine full-length CCL19 cDNA (GenBank accession number, AB163919) was inserted into the pCAG-Neo hIgG1-Fc vector (FUJIFILM Wako Pure Chemical Corporation, Osaka, Japan). Human embryonic kidney (HEK) 293 cells (NIBIOHN JCRB Cell Bank, Osaka, Japan) were cultured in Dulbecco's modified Eagle's medium (DMEM; FUJIFILM Wako Pure Chemical Corporation) supplemented with 10% heat-inactivated fetal bovine serum (FBS; Biosera, Nuaille, France) at 37°C in an atmosphere of air containing 5% CO_2. The pCAG-Neo canine CCL19-hIgG1-Fc plasmid was transfected into HEK293A cells using Lipofectamine 2000 (Thermo Fisher Scientific) according to the manufacturer's instructions. Six hours after transfection, DMEM was exchanged with serum-free medium HE100 (GMEP Inc., Kurume, Japan) including 2 mM L-glutamine. After a further incubation for 6 days, the culture supernatant was collected and purified through ultrafiltration using the Amicon Ultra-15 Centrifugal Filter Unit (Merck, Darmstadt,

Germany). Immunoblotting was conducted to confirm the presence of cCCL19-hIgG-Fc in the purified supernatant. In brief, proteins of the purified supernatant were separated by sodium dodecyl sulfate 12% polyacrylamide gel electrophoresis (SDS-PAGE) and then transferred onto a nitrocellulose membrane. One hour after blocking with 5% skim milk, the membrane was incubated with HRP-conjugated goat anti-human IgG-Fc antibody (Thermo Fisher Scientific) at 4°C overnight. Regarding signal development, an enhanced chemiluminescence reaction was conducted with ImmunoStar Zeta (FUJIFILM Wako Pure Chemical Corporation). Images were acquired using a chemiluminometer (ImageQuant LAS 500).

2.2.2. Validation of cCCL19-hIgG-Fc with canine CCR7-transfectants

Canine CCR7-transfectants were prepared using the pMX-IP Retroviral vector (provided by Kitamura, T. at the Institute of Medical Science, The University of Tokyo) containing full-length canine CCR7 cDNA (GenBank accession number, MZ209267). NIH Swiss mouse embryonic fibroblast cells (NIH3T3 cells; provided by the Institute of Development, Aging, and Cancer, Tohoku University) were retrovirally transduced. Since the pMX-IP Retroviral vector harbored the resistance gene to

puromycin, transduced NIH3T3 cells were sorted by selection medium containing 10 μg/mL puromycin (FUJIFILM Wako Pure Chemical Corporation) more than three times. After incubation with blocking buffer containing bovine (Biosera), mouse (Kohjin Bio Inc., Sakado, Japan) and rat (Merck) sera for 30 min, cells were incubated with cCCL19-hIgG-Fc at 4°C for 45 min. Cells were then washed and stained with Allophycocyanin (APC)-conjugated anti-human IgG-Fc (BioLegend, San Diego, CA, U.S.A.) as a secondary antibody at 4°C for 30 min. Purified human IgG (FUJIFILM Wako Pure Chemical Corporation) was used as an isotype control. The fluorescence of APC was detected using a flow cytometer (FACSCanto^{TM}II; BD Biosciences, Franklin Lakes, NJ, U.S.A.) and flow cytometry data were analyzed using flow cytometry software (FlowJo version 10.7.1; Becton Dickinson and Company, Franklin Lakes, NJ, U.S.A.).

2.2.3. Canine lymphoma cell lines

Three canine lymphoma cell lines, EO-1, CLC, and UL-1 cells, were employed. EO-1 cells were derived from a dog with ECTCL (22), which was developed in my laboratory. The origins of CLC and UL-1 cells were gastrointestinal lymphoma

and renal lymphoma, respectively (71). EO-1 and CLC but not UL-1 cells had shown LN metastasis in murine xenograft models (28, 71). Each cell line was cultured in RPMI 1640 (FUJIFILM Wako Pure Chemical Corporation) supplemented with 10% FBS, 1% penicillin/streptomycin, and 2 mM L-glutamine.

2.2.4 Transcription and expression analyses of CCR7

The total RNA of each canine lymphoma cell line was extracted using the RNeasy Mini Kit (QIAGEN). Genomic DNA was removed with a TURBO DNA-free Kit (Applied Biosystems, Foster, CA, U.S.A.). Total RNA was reverse transcribed to cDNA using the PrimeScript™ RT Reagent Kit (Takara Bio Inc.). The transcription of CCR7 was quantified by two-step RT-PCR (Thermal Cycler Dice Real Time System TP800; Takara Bio Inc.) using SYBR Premix Ex Taq™ II (Takara Bio Inc.). PCR primers were as follows: forward (5'-TGGTGGTGGCTCTCCTTGTC-3') and reverse (5'-AAGTTCCGCACGTCTTTCTTG-3'). Three reference genes, including CG14980, Hypoxanthine phosphoribosyltransferase 1 (HPRT1), and TBP, were selected by GeNorm and Bestkeeper among nine candidate reference genes (B2M, CG14980, GAPDH, HPRT1, RPL13A, RPL32, RPS18, ACTB, and TBP) (27, 71). Amplification

consisted of a first period of activation (95°C for 10 sec) followed by 40 cycles of a PCR reaction (95°C for 5 sec and 60°C for 30 sec) and dissociation (95°C for 15 sec, 60°C for 30 sec, and 95°C for 15 sec). Each PCR reaction included samples without reverse transcription, which were not amplified in chapter 2. The geometric mean of the cycle threshold (Ct) values of the three reference genes were subtracted from the Ct values of CCR7 (ΔCt). All samples were examined in duplicate, and the mean value of ΔCt was calculated. The relative transcription level of CCR7 was calculated by $2^{-\Delta Ct}$, resulting in the evaluation of samples as n-fold differences from the mean value of the three reference genes. The experiment was independently implemented three times.

The detection of CCR7 protein in EO-1, CLC, and UL-1 cells was conducted by flow cytometry using cCCL19-hIgG-Fc in the same manner as in canine CCR7-transfectants described above.

2.2.5. Chemotaxis assay

A chemotaxis assay was performed in a 24-transwell plate with a 5-μm pore insert (Corning Inc., Corning, NY, U.S.A.). Canine recombinant CCL19 (Kingfisher Biotech Inc., Saint Paul, MN, U.S.A.) and mouse recombinant CCL19 (Prospec, Ness-

Ziona, Israel) were diluted in RPMI 1640 from 0.1 to 500 nmol/l, and 600 µl of the diluted solution was placed in the lower chamber. EO-1 and UL-1 cells were resuspended in RPMI 1640 at 1×10^7 cells/ml, and 100 µl of each cell suspension was added to the upper chamber. After an incubation for 3 hours at 37°C under 5% CO_2, the number of migrated cells in the lower chamber was counted. The assay was performed in duplicate.

2.2.6. Statistical analysis

The relative mRNA levels of CCR7 in cell lines were statistically analyzed by the Dunn's test. A value of $P < 0.05$ was considered significant. Statistical analyses were performed using the JMP 13.2.0 program (SAS Institute).

2.3. Results

2.3.1. Validation of cCCL19-hIgG-Fc

Immunoblotting detected a single band near 37 kDa corresponding to the expected molecular weight of canine CCL19 combined with the human IgG-Fc region in the purified supernatant (Figure 2-1a). A flow cytometric analysis showed that cCCL19-hIgG-Fc bound to NIH3T3 cells transfected with canine CCR7, but not to non-transfectants (Figure 2-1 b).

2.3.2. Transcription and expression of CCR7

The qRT-PCR analysis showed that CCR7 mRNA expression levels were significantly higher in EO-1 cells than in UL-1 cells (Figure 2-2 a). The flow cytometric analysis also revealed that positive staining was moderate in EO-1 cells and dim in CLC cells, but almost negative in UL-1 cells (Figure 2-2 b).

2.3.3 Chemotactic activity of CCR7

In the chemotaxis assay, the number of migrated EO-1 cells increased in proportion to the concentration of both canine and mouse CCL19. In contrast, UL-1 cells showed no increase in the number of migrated cells (Figure 2-3).

2.4. Discussion

In canine studies, anti-human antibodies have been used to detect chemokine receptors, such as CCR4 and CCR9 (47, 48). However, there have been no antibodies reactive to canine CCR7, which prompted me to focus on the receptor-ligand binding assay using the fusion protein cCCL19-hIgG-Fc. Since the specificity of CCL19-hIgG to canine CCR7 was previously reported to be unclear (24), I initially validated the specificity by using the canine CCR7-transfectants. The results obtained demonstrated that cCCL19-hIgG-Fc specifically bound to canine CCR7.

The results of transcription and expression analyses showed that the expression of CCR7 varied among canine lymphoma cell lines. I employed EO-1 cells as the cell line showing the highest expression levels of CCR7 and UL-1 cells as that with the lowest for the chemotaxis assay to evaluate the function of canine CCR7. The results of the assay indicated the active chemotaxis of EO-1 cells not only to canine but also to mouse recombinant CCL19, which ensures mouse models xenografted with canine cell lines to evaluate the roles of canine CCR7 in tumor cell dynamics. Previous studies reported the metastasis of regional LNs in 4/4 and 3/4 mice xenografted with EO-1 or CLC cells, respectively (28, 71), but not in mice xenografted with UL-1 cells

(71). Since the major function of CCR7 is homing to LNs, the metastasis of regional LNs in these mouse models appeared to be related to the expression of CCR7 in xenografted tumor cells. Further studies including the knockdown or KO of CCR7 in EO-1 and CLC cells are required to clarify the involvement of canine CCR7 in metastasis.

In conclusion, I revealed that the canine ECTCL cell line expressed functional CCR7. The results of chapter 2 demonstrated that the cCCL19-hIgG-Fc fusion protein was specific to detect canine CCR7, which contributes to further studies to investigate the pathophysiological roles of CCR7 in metastasis of canine ECTCL.

2.5. Table and Figure

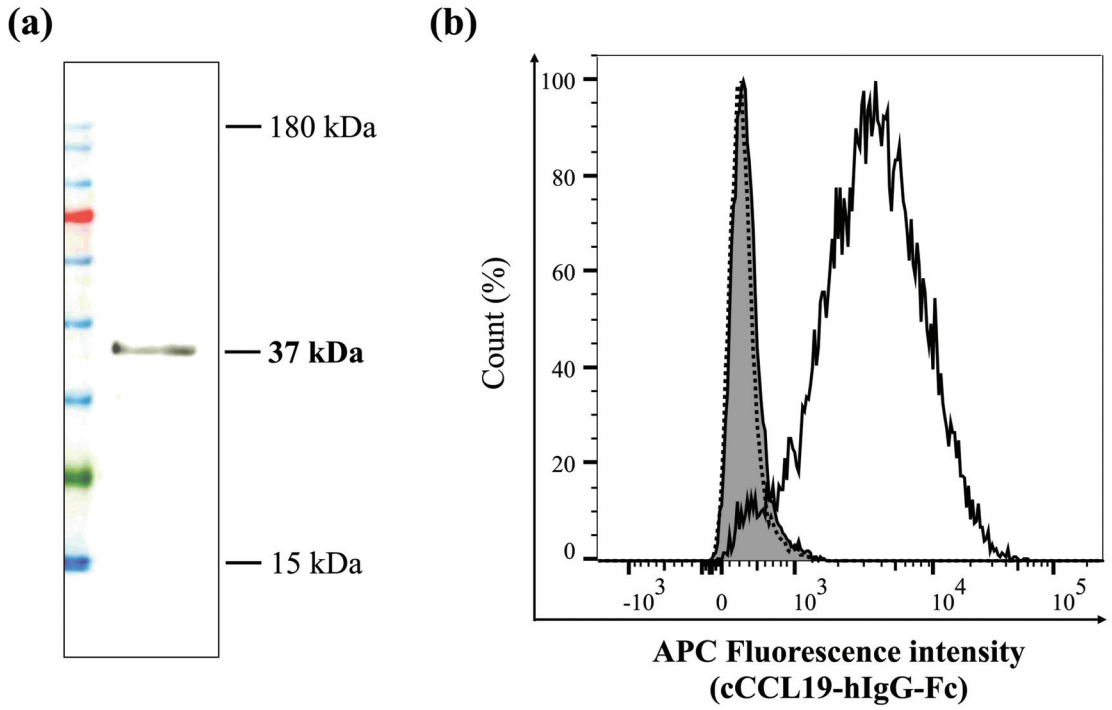

Figure 2-1. Immunoblotting and flow cytometric analysis of cCCL19-hIgG-Fc.

(a) Immunoblotting using an anti-human IgG-Fc antibody in the purified culture supernatant of HEK293 cells transfected with the pCAG-Neo cCCL19-hIgG1-Fc plasmid.

(b) The flow cytometric analysis showed that cCCL19-hIgG-Fc bound to canine CCR7-transfectants (white area), but not to non-transfectants (dotted line). The grey area represented the isotype control.

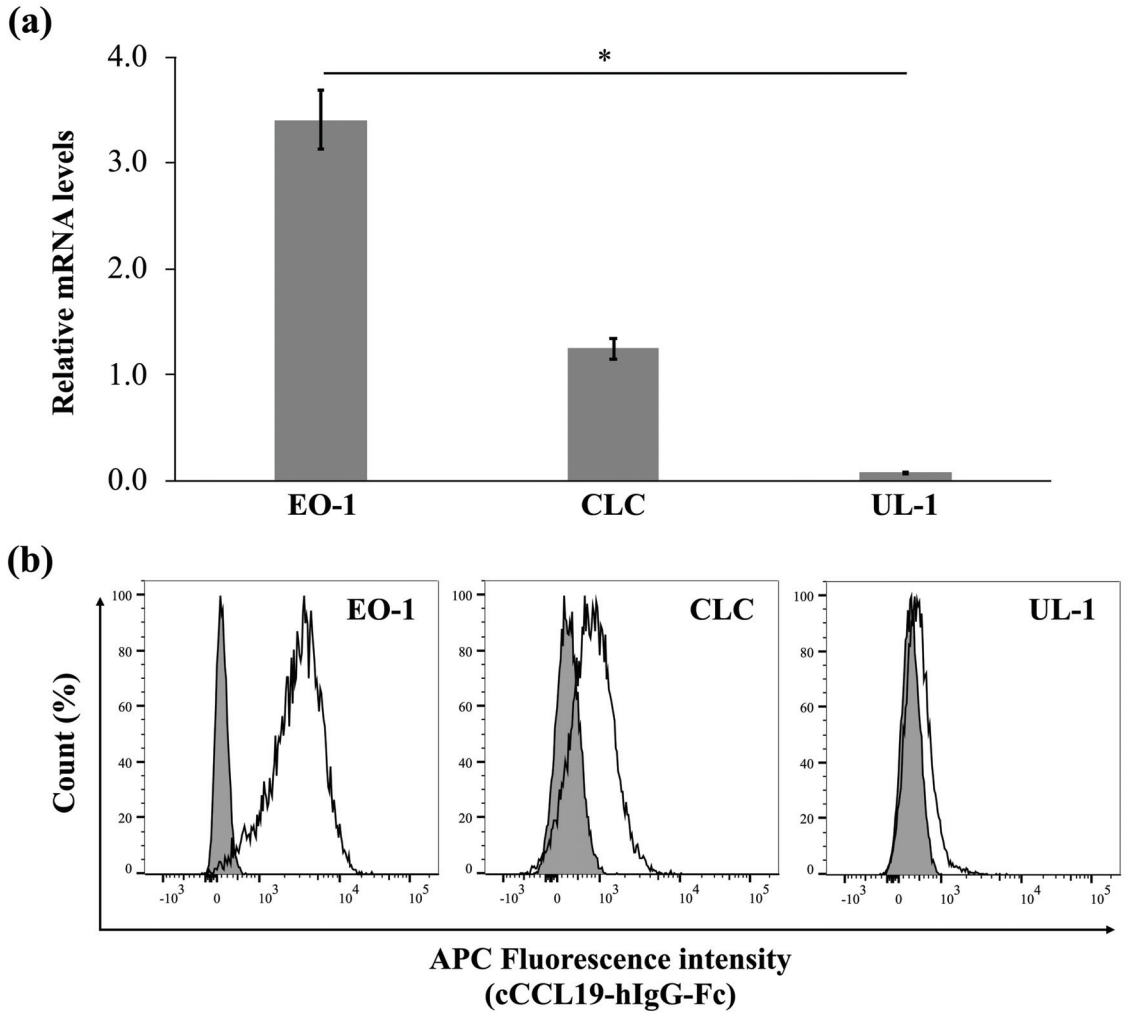

Figure 2-2. Expression analysis of CCR7 in canine lymphoma cell lines (EO-1, CLC, and UL-1).

(a) The expression of canine CCR7 mRNA was shown as a relative quantity. Results were shown as the means ± SD of three independent experiments. *$P < 0.05$ by Dunn's test. (b) The histogram showed staining intensities by the isotype control (grey area) and cCCL19-hIgG-Fc (white area).

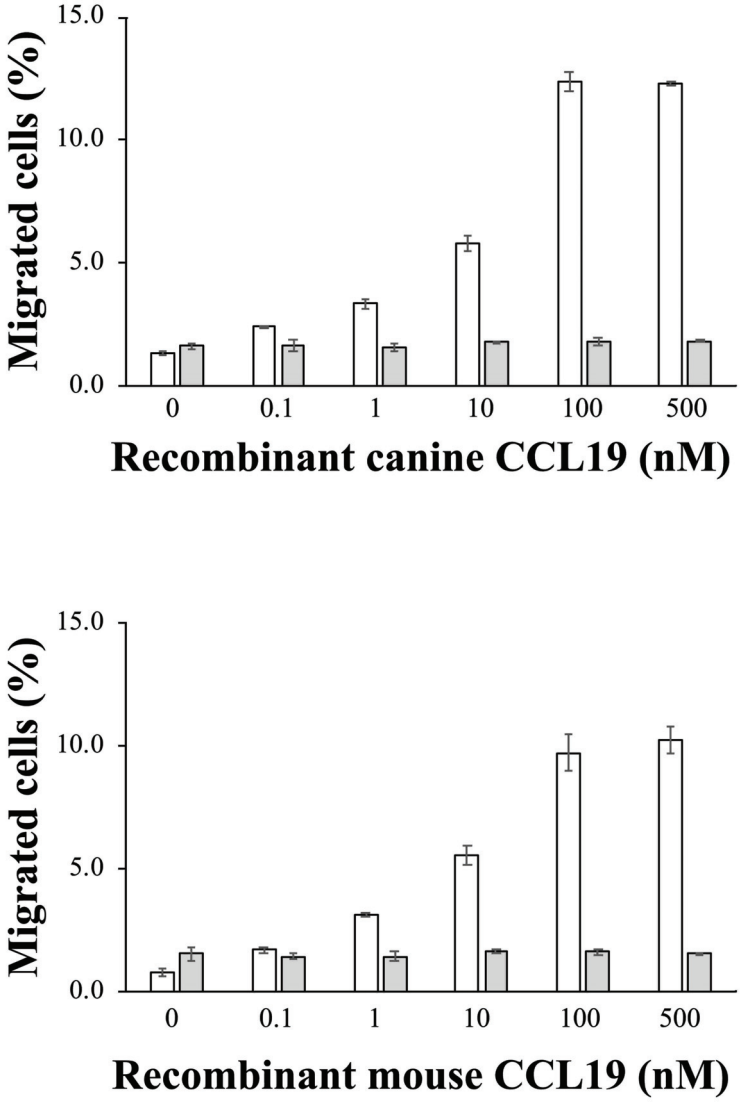

Figure 2-3. Chemotaxis assay using canine and mouse recombinant CCL19.

White bars represented EO-1 cells, and grey bars represented UL-1 cells. Results were shown as the means ± SD of two independent experiments.

Chapter 3

Evaluation of pathophysiological roles of chemokine receptor 4 and 7 in a canine epitheliotropic cutaneous T-cell lymphoma model

3.1. Introduction

Cancer metastasis consists of a multi-stage process that includes the migration and proliferation of tumor cells (63). Since cell migration is regulated by interactions between chemokines and chemokine receptors (42), numerous studies have examined the roles of chemokines in cancer metastasis. An initial study revealed that CXC chemokine receptor (CXCR) 4 was highly expressed in human breast cancer. Furthermore, CXC chemokine ligand 12, the ligand for CXCR4, was preferentially expressed in metastatic organs, such as the lungs and LNs, suggesting the involvement of chemokines in organ-specific metastasis. In murine xenografted models, a CXCR4-blocking antibody inhibited lung and LN metastasis. Other chemokine receptors, including CCR6, CCR9, and CXCR3, were also shown to be involved in the metastasis of colorectal cancer (20), melanoma (59), and colon cancer (34), respectively. A study on dogs demonstrated that the transcription levels of CXCR3, CXCR4, CXCR7, and CCR9 were significantly higher in metastatic mammary carcinoma than in non-metastatic mammary carcinoma (1). Canine cell lines of leukemia and osteosarcoma also expressed functional CCR9 (47) and CXCR4 (14); however, the relationship between each chemokine receptor and organ-specific metastasis remains unclear in

dogs.

Cell proliferation is induced by various molecules, including growth factors, colony-stimulating factors, interleukins, tumor necrosis factors, and chemokines (3). The roles of chemokines in cell proliferation have been intensively investigated in tumors. In human glioblastoma cell lines expressing CCR5, the stimulation of CCL5 induced cell proliferation with an increase in intracellular phosphor-Akt (p-Akt) (85). Since the knockdown of CCR5 decreased cell proliferation and p-Akt in the presence of CCL5, the Akt pathway was most likely involved in cell proliferation induced by CCL5 and CCR5. Similarly, tumor growth was suppressed by the inhibition of other chemokine receptors, such as CXCR3 in hepatocellular carcinoma (58), CXCR4 in breast cancer (26), and CCR10 in glioma (8). These findings suggest that chemokines play an essential role in tumor cell proliferation, which has not yet been examined in dogs.

A previous study on canine ECTCL showed that the transcription levels of CCR4 and CCR7 were significantly higher in skin lesions than in normal skin (9). A canine ECTCL cell line also expressed CCR4 (22) and CCR7 (32), exhibiting chemotactic activity to their ligands. In human and murine studies, activated keratinocytes and dendritic cells produced the ligands for CCR4, such as CCL17 (73,

74) and CCL22 (75), which promoted the skin tropism of CCR4-positive cells (82). Murine CCR7 facilitated cell migration from peripheral tissues to LNs via lymphatic vessels at which CCL19 and CCL21, ligands for CCR7, were abundant (5). These findings indicate that CCR4 and CCR7 are involved in epitheliotropism and LN metastasis, respectively, in canine ECTCL. In mice xenografted with human breast cancer cell lines, tumors of CCR4-overexpressing cells were more significantly increased than those in mice transferred with wild-type (WT) control cells (44). CCL21 enhanced *in vitro* dose-dependent cell proliferation in human lung and bladder cancer cells (51, 77), which was inhibited by the knockdown of CCR7 or a CCR7-blocking antibody. Therefore, the roles of CCR4 and CCR7 in cell proliferation also need to be investigated in canine ECTCL.

The cell line EO-1 has been established for canine ECTCL in my laboratory (22), and xenografted mice developed both skin lesions and systemic metastasis, similar to dogs with ECTCL . In chapter 3, I examined the pathophysiological roles of CCR4 and CCR7 in tumor cell migration and proliferation in canine ECTCL.

3.2. Materials and Methods

3.2.1. Cell line

The canine ECTCL cell line EO-1 was cultured in 75 cm^2 of RPMI 1640 supplemented with 10% heat-inactivated fetal bovine serum, 2 mM L-glutamine, and 1% penicillin/streptomycin at 37°C in a humidified atmosphere of 5% CO_2. The culture medium was changed three times each week. As the cell line validation, the doubling time, morphology, and surface markers, such as CD3, CD8, TCR-gamma delta, CCR4, and CCR7, were confirmed to be identical as previously reported (32).

3.2.2. KO of chemokine receptors in EO-1

The CRISPR/Cas9 system was used for the KO of the CCR4 or CCR7 genes in EO-1 cells. The sequences of guide RNAs (gRNAs) for canine CCR4 and CCR7 were designed using CHOPCHOP (43) and CRISPR direct (56). gRNAs were as follows: CCR4: 5'-TAAGCCTTGCACCAAAGAAG-3' and CCR7:5'-AGATACGTACCTGCTCAACC-3'. gRNAs were inserted into the plasmid pGuide-it

ZsGreen vector (Takara Bio Inc.). The plasmid vector was then transfected into EO-1 cells by electroporation using the Neon Transfection System (Thermo Fisher Scientific). Transfected EO-1 cells were sorted based on green fluorescence by Cell Sorter SH800S (Sony; Tokyo, Japan) and re-cultured. After a further incubation for three weeks, CCR4KO and CCR7KO EO-1 cells were sorted according to the disappearance of CCR4 and CCR7 expression, respectively.. Regarding the features of EO-1 cells described above, no changes were detected in CCR4KO or CCR7KO EO-1 cells.

To evaluate the efficacy of KO on cell migration, a chemotaxis assay was conducted in a 24-transwell plate with a 5-μm pore insert (Corning Inc.). In brief, mouse recombinant CCL17 (Bio Legend) and CCL19 (Prospec) were diluted in RPMI 1640 from 0.1 to 500 nmol/L, and 600 μL of the diluted solution was placed in the lower chamber. WT, CCR4KO, and CCR7KO EO-1 cells were resuspended in RPMI 1640 at 1×10^7 cells/mL, and 100 μl of each cell suspension was added to the upper chamber. After an incubation at 37°C for 3 hours under 5% CO_2, the number of migrated cells in the lower chamber was counted. The assay was independently performed twice.

3.2.3. Xenograft mouse model

Seven-week-old female NOD SCID mice were purchased from Charles River Laboratories Japan, Inc.. Mice were maintained under specified pathogen-free conditions and fed autoclaved food and water. As an adaptation period, mice were observed for one week before xenograft implantation.

Mice were divided into three groups (WT, CCR4KO, and CCR7KO). A total of 1×10^8 EO-1 cells were subcutaneously injected into the left thigh of four mice per group under anesthesia with the inhalation of isoflurane (Pfizer, Tokyo, Japan). The general condition of mice was monitored daily with measurements of body weight every 3 days. Mice were sacrificed 28 days after xenograft implantation. Tissue samples from skin, LNs, spleen, lung, liver, kidney, heart, and bone marrow were fixed in 10% neutral buffered formalin and embedded in paraffin for immunohistochemistry (IHC). Peripheral blood was collected in a heparin-containing syringe by cardiac puncture. Subcutaneous nodular sizes were measured under the skin incision. All procedures above were approved by the Institutional Animal Care and Use and Clinical Ethics Committees of Gifu University (Accession number: 2020-254).

3.2.4. IHC

Paraffin-embedded tissue sections (thickness of 3 μm) were pretreated in antigen retrieval solution (Dako; Glostrup, Denmark) by autoclaving at 121°C for 15 min followed by an incubation with either rabbit anti-human CD3 antibody (C7930, Sigma-Aldrich; Saint Louis, MO, U.S.A.)(28, 54) or normal rabbit IgG isotype control (FUJIFILM Wako Pure Chemical Corporation). Since T-cells cannot be recognized in three-month-old SCID mice (62), CD3-positive cells represent EO-1 cells in this study. After an overnight incubation at 4°C, sections were treated with a horseradish peroxidase-labeled polymer (Dako). The chromogen 3,30-diaminobenzidine (DAB, Dako) was used for the visualization of immunolabelling, followed by counterstaining with hematoxylin. Slides were observed with an optical microscope (DM2500, Leica; Wetzlar, Germany).

3.2.5. Quantitative evaluation of EO-1 cells in tissues

The distribution of EO-1 cells in each tissue was quantified using ImageJ Fiji software ver. 2.3.0 (10, 61) as previously described (19, 31, 41). In brief, hematoxylin (non-EO-1 cell region) and DAB staining (EO-1 cell region) were separated from IHC

images by a color deconvolution procedure. The area of each stain was then measured. The area of infiltrated EO-1 cells was shown as a percentage of the DAB area in the hematoxylin area.

3.2.6. Quantitative evaluation of EO-1 cells in peripheral blood

The white blood cells of mice were isolated from 100 μL of peripheral blood by lysing buffer (BD Biosciences), followed by an incubation with FITC-conjugated mouse anti-canine CD3 antibody (clone CA17.2A12, Bio-Rad Laboratories; Hercules, CA, U.S.A.) in washing buffer at 4°C for 30 min. An appropriate isotype control (FITC-conjugated mouse IgG1, clone MOPC-21, Bio Legend) was used. The percentage of EO-1 cells, which were positive for CD3, in white blood cells was evaluated by a flow cytometer (FACS Canto II).

3.2.7. Cell proliferation assay

Cell proliferation was examined using Cell Counting Kit-8 (CCK-8, FUJIFILM Wako Pure Chemical Corporation) as previously reported (77). In brief, WT,

CCR4KO, and CCR7KO EO-1 cells were seeded on 96-well plates at 2×10^4 cells/100 μL and treated with 100 ng/mL of recombinant murine CCL17, CCL19, CCL21 (PEPRO TECH; Cranbury, NJ, U.S.A.), or CCL22 (PEPRO TECH) for 0, 24, 48, or 72 hours. After the treatment, a coloring reagent of CCK-8 was added to each well according to the manufacturer's instructions and incubated at 37°C for 2 hours. The optical density value of each well was measured using a microplate reader (Bio-Rad) at a wavelength of 450 nm. Cell proliferation at each time point was shown as a percentage relative to 0 hours. The assay was independently repeated three times.

3.2.8. Statistical analysis

Dunnett's test was conducted to compare the distribution of EO-1 cells, the body weight of mice, and the size of nodules and LNs between the WT and KO groups. Cell proliferation was also compared between control cells and cells treated with chemokines by Dunnett's test. A value of $P < 0.05$ was considered to be significant. Statistical analyses were performed using the JMP ver. 13.2.0 (SAS Institute).

3.3. Results

3.3.1 Validation of KO

Flowcytometric analysis demonstrated that the proportion of both CCR4KO and CCR7KO EO-1 cells reached more than 99% (Figure 3-1). In the chemotaxis assay, neither CCR4KO nor CCR7KO EO-1 cells showed active chemotaxis to each chemokine ligand (Figure 3-2).

3.3.2. Xenograft mouse model

All mice in each group gained weight until day 24 after xenograft implantation. Only the weight of the WT group was significantly lower than those of the other groups on day 27 (Figure 3-3).

3.3.3. Distribution of xenografted EO-1 cells

In all tissues and blood, the proportion of EO-1 cells was significantly lower

in the CCR4KO and CCR7KO groups than in the WT group (Figure 3-4). In tissues, EO-1 cells frequently localized around blood vessels. Normal lung structures disappeared due to an increase of EO-1 cells in the WT group (Figure 3-5). Iliac lymphadenopathy was observed in 4/4, 3/4, and 3/4 mice in the WT, CCR4KO, and CCR7KO groups respectively, whereas mesenteric, inguinal, and bronchial lymphadenopathies were only detected in the WT group (Table 3-1). Iliac LNs in the WT group (diameter: 7.9 ± 0.22 mm) were significantly larger ($P < 0.001$) than those in the CCR4KO (5.0 ± 0.71 mm) and CCR7KO (5.0 ± 0.41 mm) groups. Lymphadenopathy was attributed to the massive infiltration of EO-1 cells.

3.3.4. Subcutaneous nodule formation

All mice developed nodules in the subcutis at which EO-1 cells had been injected (Figure 3-6). Nodules were significantly smaller in the CCR4KO and CCR7KO groups than in the WT group (Figure 3-7).

3.3.5. Cell proliferation assay

The average increase in cells treated with chemokine ligands was 301% in 48 hours, which was significantly higher than that of control cells at 246% (Figure 3-8 a). In CCR4KO and CCR7KO cells, no significant differences were observed in cell proliferation among the groups (Figure 3-8 b, c).

3.4. Discussion

Results from flowcytometric analysis and chemotaxis assay in CCR4KO and CCR7KO EO-1 cells showed that the procedure of KO was appropriately conducted, whereas there were no changes in the features of EO-1 cells including cell surface markers, morphology, and doubling time. These results suggested that the KO cells enabled various studies to investigate the pathophysiological roles of CCR4 and CCR7 in ECTCL by comparing to the WT cells.

Immunohistochemical and flow cytometric analyses revealed that the proportion of xenografted EO-1 cells in tissues and blood was significantly lower in the CCR4KO and CCR7KO groups than in the WT group. Large amounts of infiltrating EO-1 cells may induce multiple organ failure contributing to the decreased body weight in the WT group. Histopathological observations of the WT group also showed that EO-1 cells localized around blood vessels in metastatic tissues. Previous studies revealed that tumor cells increased in perivascular sites after extravasation when injected intravascularly (6, 39). Collectively, these findings and my results indicate that EO-1 cells infiltrate metastatic organs from blood vessels; therefore, the proportion of EO-1 cells in tissues has been attributed to the number of EO-1 cells in blood. No significant

differences were observed in the types of metastatic organs among groups, indicating that chemotaxis does not affect metastatic organs once EO-1 cells enter the circulation.

LNs are a crucial immune site for the antigen presentation of dendritic cells and the activation of naïve lymphocytes. Naïve lymphocytes enter LNs via high endothelial venules; however, recent studies showed that activated lymphocytes returned to LNs from peripheral tissues through draining lymph vessels (5, 70). Cancer cells have been shown to exploit draining lymph vessels for their exit from primary locations and infiltration into LNs (33). Therefore, I focused on the migration of EO-1 cells into LNs. In chapter 3, LNs were only visible when enlarged with the infiltration of EO-1 cells. In the WT group, iliac lymphadenopathy was detected in all four mice, whereas the enlargement of mesenteric, inguinal, and bronchial LNs was recognized in 3/4, 2/4, and 1/4 mice, respectively. In the CCR4KO and CCR7KO groups, lymphadenopathy was only observed in iliac LNs. Therefore, iliac lymphadenopathy was detected in the WT, CCR4KO, and CCR7KO groups. Since iliac LNs are sentinel LNs for the thigh, into which EO-1 cells were injected, it is plausible that EO-1 cells left the subcutis and entered iliac LNs, followed by the circulation. The size of iliac LNs was significantly smaller in the CCR4KO and CCR7KO groups, which may have reduced the number of EO-1 cells in blood. Therefore, the reduction in chemotaxis to

sentinel LNs appeared to contribute to the suppression of subsequent systemic metastasis in the CCR4KO and CCR7KO groups. The most well-described chemokines for cell migration to LNs are CCL19 and CCL21 (5); however, CCL22 was also shown to be produced in large amounts by dendritic cells in LNs (57, 69), facilitating the recruitment of CCR4-positive T-cells to LNs. In the CCR4KO and CCR7KO groups, an interruption between CCR4 or CCR7 and their ligands appeared to inhibit the migration of EO-1 cells from the subcutis to sentinel iliac LNs.

Subcutaneous nodule formation was significantly less in the CCR4KO and CCR7KO groups than in the WT group. To establish whether chemokines facilitated tumor growth, I conducted a cell proliferation assay, the results of which indicated that chemokine ligands accelerated the proliferation of EO-1 cells, suggesting that CCR4 and CCR7 were also involved in tumor growth in canine ECTCL murine models. However, it is uncertain whether the proportion of tumor cells in the metastatic organs was attributed to the amounts of migrated cells or to the cell proliferation enhanced by chemokines. Further studies are necessary to investigate the proliferation of tumor cells in metastatic tissues by evaluating cellular markers for proliferation. In a previous study on the role of the downstream signaling of CCL17/CCR4 in the proliferation of human cervical cancer cells, the inhibition of cell proliferation by the blockade of various

signaling molecules, including Akt, JNK, STAT3, STAT5, MAPK, ERK, and NFκB, under a CCL17 stimulation was examined. The findings obtained showed that the blockade of only JNK or STAT5 decreased cell proliferation (45). In human lung cancer cells, CCL21 was shown to induce cell proliferation with an increase in p-ERK (77). Furthermore, the Akt pathway was involved in the cell proliferation of glioblastoma by CCL5/CCR5 (85). Collectively, these findings suggest that signaling pathways with JNK, STAT5, ERK, and Akt are involved in cell proliferation by canine CCR4 and CCR7.

In conclusion, I demonstrated that CCR4 and CCR7 facilitated the migration of EO-1 cells to sentinel LNs, which contributed to subsequent systemic metastasis. The results of chapter 3 indicated that CCR4 and CCR7 also induced cell proliferation *in vitro* and *in vivo*. Since systemic metastasis and local tumor growth are both serious issues in cancer, not just in ECTCL, targeting chemokine receptors will be a novel therapeutic option.

3.5. Table and Figure

	WT	CCR4KO	CCR7KO
Iliac	**4**	**3**	**3**
Mesenteric	**3**	**0**	**0**
Inguinal	**2**	**0**	**0**
Bronchial	**1**	**0**	**0**

Table 3-1. The number of mice with lymphadenopathy in each LN.

LNs were detected only when enlarged with the infiltration of EO-1 cells. Iliac lymphadenopathy was recognized in the WT, CCR4KO and CCR7KO groups, whereas other lymphadenopathies was observed only in the WT group.

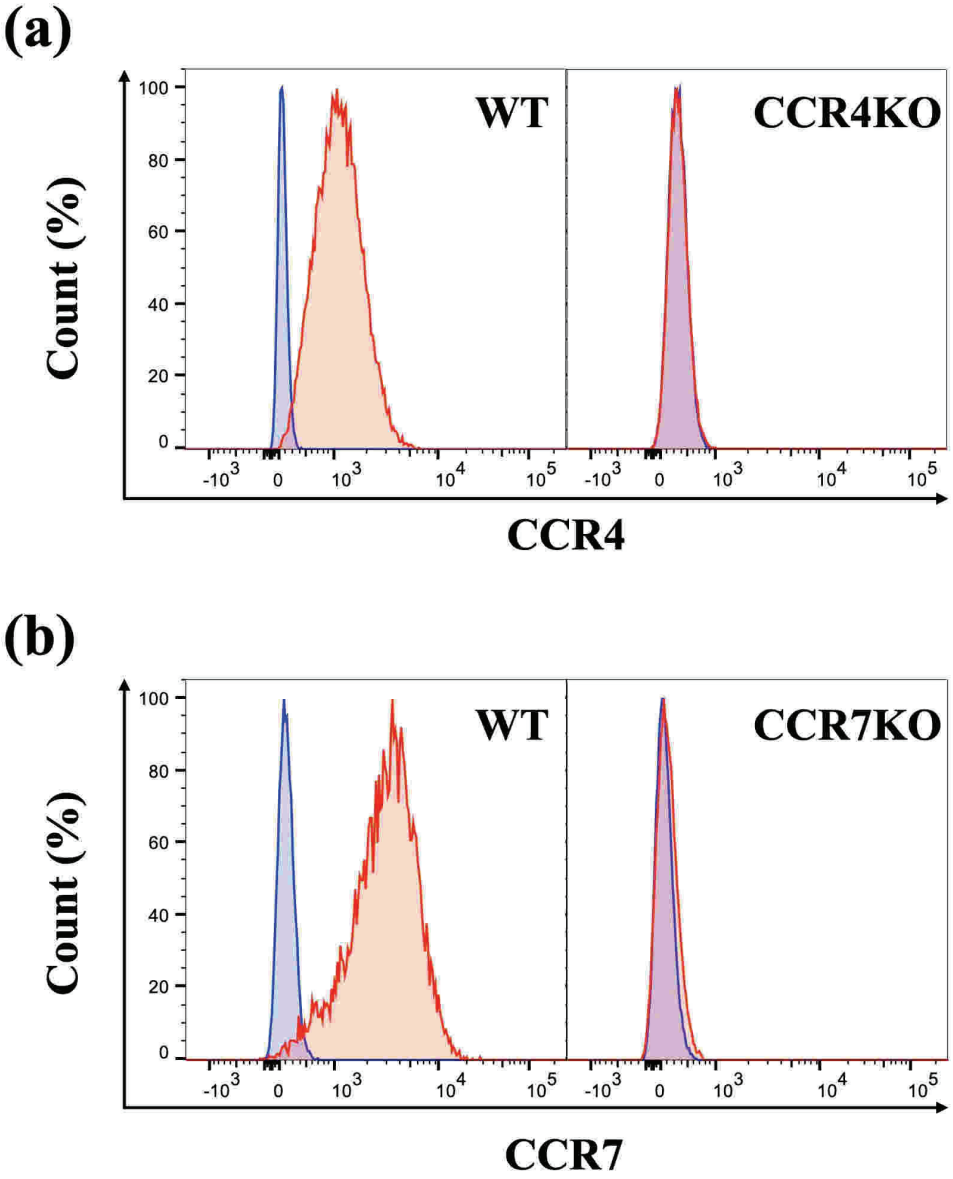

Figure 3-1. Expression analysis of CCR4 or CCR7 in WT and KO cells.

The histogram showed intensities by isotype controls (blue area) and antibodies (red area) for CCR4 (a) or CCR7 (b).

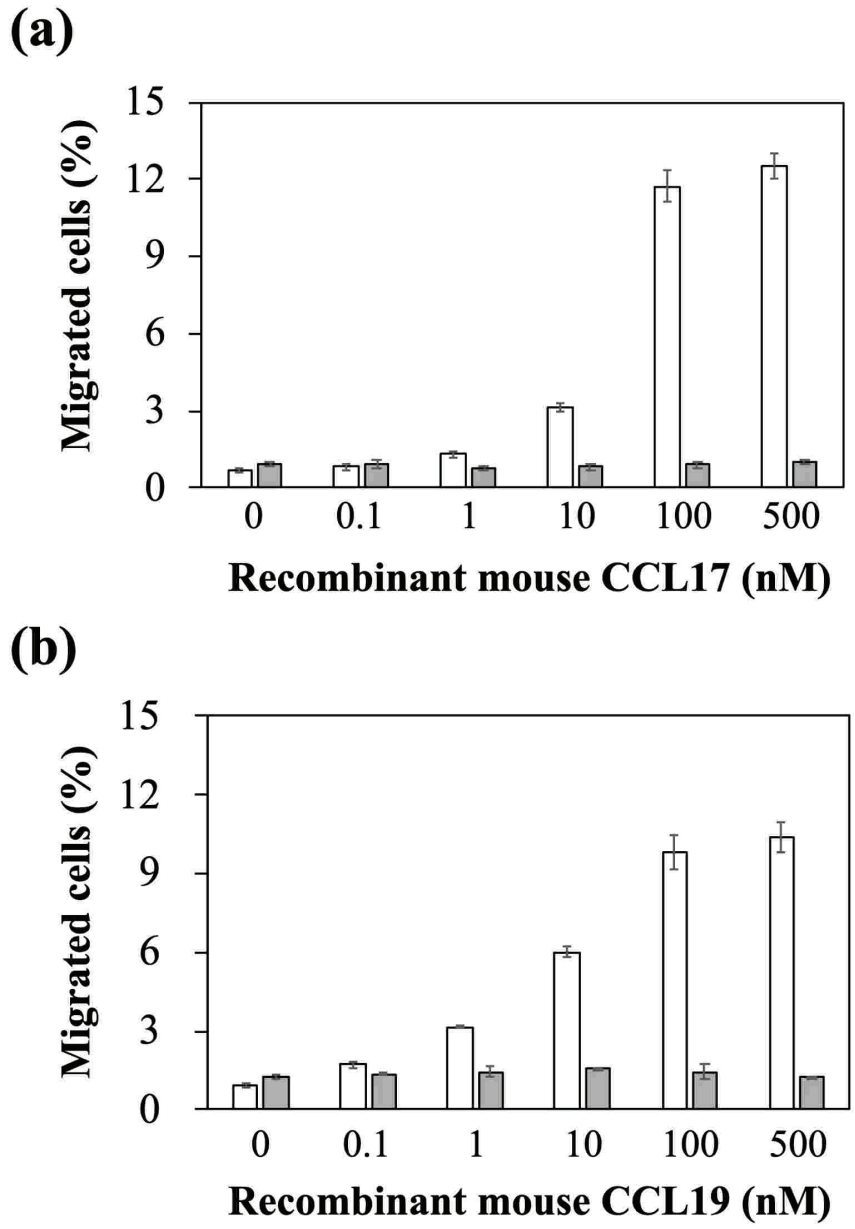

Figure 3-2. Chemotaxis assay using recombinant mouse CCL17 or CCL19.

White bars represented WT cells. Grey bars were CCR4KO (a) and CCR7KO (b) cells.

Results were shown as the means ± SD of two independent experiments.

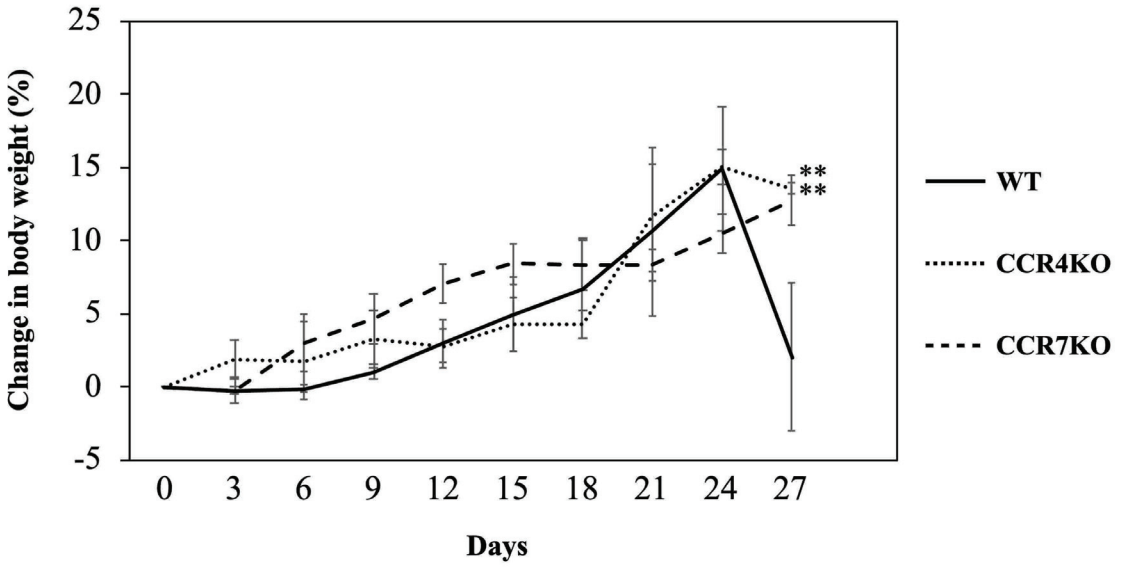

Figure 3-3. Changes in the body weight of mice based on day 0 (the date of xenograft implantation).

Data were shown as the means ± SD of four mice. The WT group was compared with CCR4KO and CCR7KO groups by Dunnett's test (**$P < 0.01$).

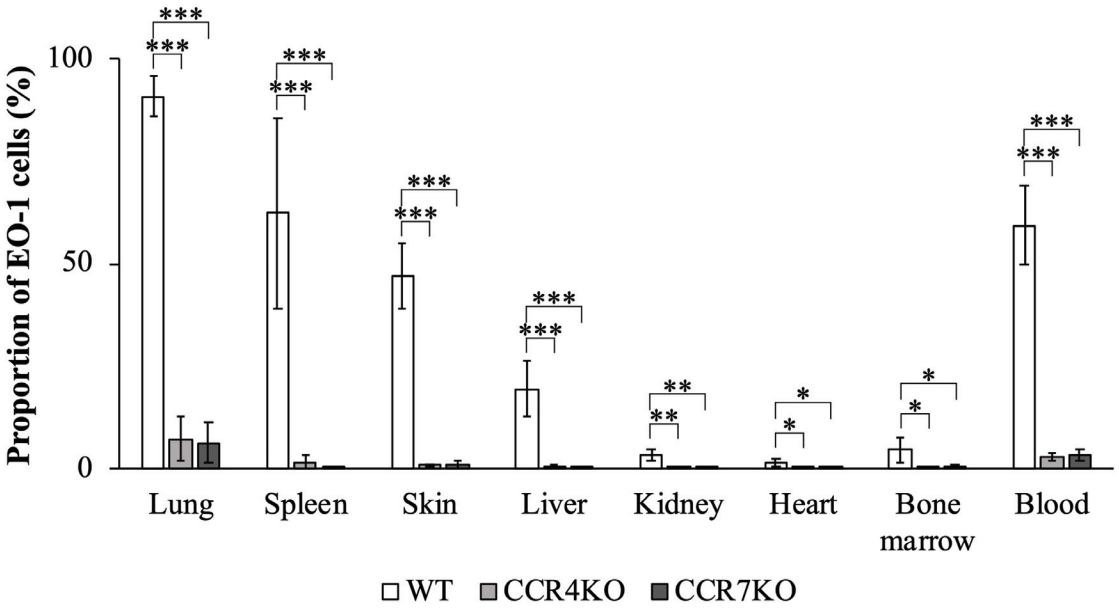

Figure 3-4. The proportion of xenografted EO-1 cells in tissues and blood.

Each bar represented the mean ± SD of four mice in the WT, CCR4KO, and CCR7KO groups. *$P < 0.05$, **$P < 0.01$, ***$P < 0.001$ by Dunnett's test.

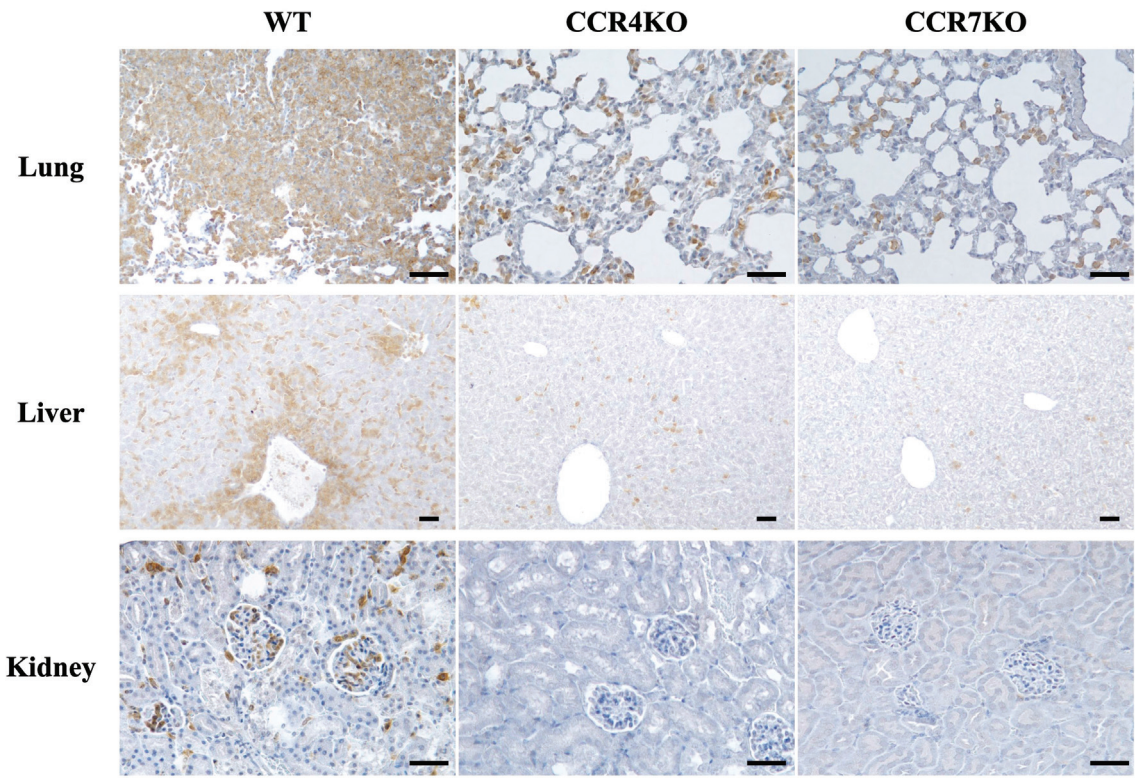

Figure 3-5. Representative immunohistochemical images of the lung, liver, and kidney.

EO-1 cells were shown as DAB-stained CD3-positive cells. Scale bars represented 50 μm.

Figure 3-6. Representative images of subcutaneous nodules.

A subcutaneous nodule was formed at the left thigh of the xenograft site in all mice.

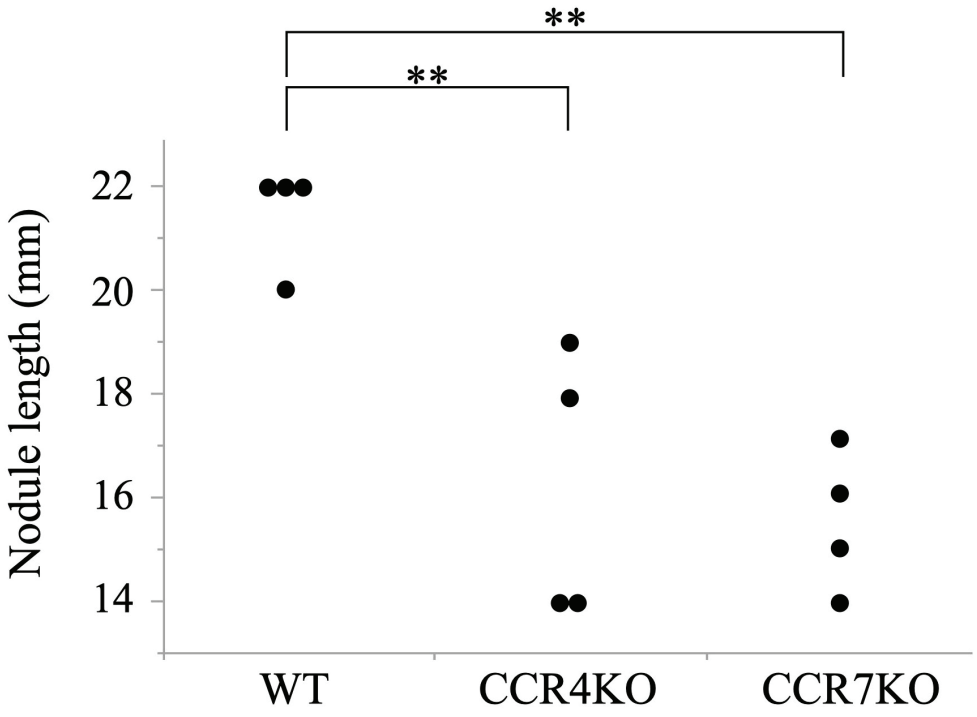

Figure 3-7. The major axis length of subcutaneous nodules. $^{**}P < 0.01$ by Dunnett's test.

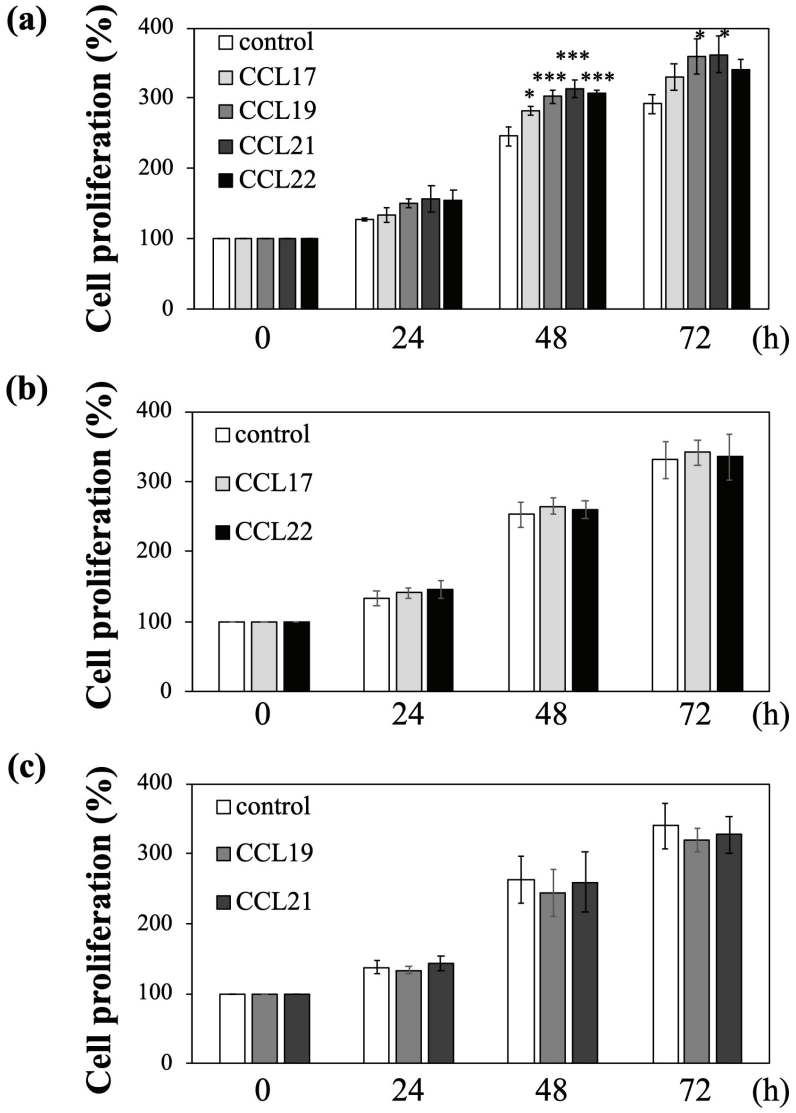

Figure 3-8. Effects of chemokine ligands on the proliferation of EO-1 cells.

(a) WT EO-1 cells treated with vehicle (control) or CCL17, CCL19, CCL21, or CCL22. (b) CCR4KO EO-1 cells treated with vehicle or CCL17 or 22. (c) CCR7KO EO-1 cells treated with vehicle or CCL19 or 21. Each bar represents the mean ± SD of three independent experiments. Cells treated with chemokines were compared with control cells by Dunnett's test (*$P < 0.05$, ***$P < 0.001$).

General Conclusion

Canine ECTCL is an intractable disease characterized by various skin lesions and poor prognosis. Definitive causes of death have not been elucidated; however, dissemination of neoplastic T-cells, such as formation of multiple skin lesions and metastasis to LNs or distant organs, is considered a crucial prognostic factor (7). Several studies on human ECTCL have shown clonal heterogeneity with multiple clones of neoplastic T-cells being observed in different skin lesions from the same patients (29, 72), which may explain the diversity in skin lesions. In contrast, identical clones of neoplastic T-cells were recognized in different skin lesions from canine ECTCL (35), indicating the systemic migration of identical neoplastic T-cells. Further investigation on the clonality and its association with skin lesions is necessary. The migration of lymphocytes is physiologically regulated by the interaction between chemokines and chemokine receptors. In canine ECTCL, CCR4 and CCR7 were highly translated in skin lesions (9). These findings indicate CCR4 and CCR7 play an important role in the migration of neoplastic T-cells. Therefore, I carried out a series of studies to investigate the association between clonality and skin lesions, and to reveal the pathophysiological roles of CCR4 and CCR7 in canine ECTCL.

In chapter 1, I revealed the clonal heterogeneity of cutaneous neoplastic T-cells, which was not associated with the clinical or histopathological features of skin lesions. On the other hand, I also demonstrated identical clones in different skin lesions and peripheral blood of some dogs with ECTCL, suggesting the systemic migration of neoplastic T-cells, which required further investigation to elucidate mechanisms.

In chapter 2, I validated the specificity of a detection tool for canine CCR7, cCCL19-hIgG-Fc, to evaluate the expression of CCR7 in a canine ECTCL cell line EO-1. The cCCL19-hIgG-Fc was confirmed to be specific to detect canine CCR7 by using CCR7-transfectants. It was also shown that EO-1 cells expressed functional CCR7, which exhibited the active chemotaxis to both canine and murine ligands.

In chapter 3, I evaluated the roles of CCR4 and CCR7 in a mouse model xenografted with EO-1 cells. The results demonstrated that the dissemination of tumor cells was significantly inhibited in the CCR4 and CCR7 KO groups. Subcutaneous nodule formation at the xenograft site was also less in the KO groups, which suggested CCR4 and CCR7 induced not only the migration but also the proliferation of tumor cells.

In conclusion, my doctoral study indicated that systemic metastasis and local tumor growth in canine ECTCL were enhanced by CCR4 and CCR7. Prospective studies should be conducted to investigate whether CCR4 and CCR7 can be used as novel therapeutics or prognostic factors which may lead to further classification for canine ECTCL.

Acknowledgments

First, I express my deepest gratitude and heartfelt thanks to my main supervisor, Professor Dr. Sadatoshi Maeda (Gifu University). He always provided me with investigational opportunities, valuable advice, kind guidance, support, generous encouragement and critical review throughout the doctoral course, sometimes strict, sometimes like a father. Thanks to his dedicated instruction, I can foster logical thinking power.

I also express my special thanks to faculties. Drs. Hiroaki Kamishina (Gifu University), Munetaka Iwata (Gifu University), Naohito Nishii (Gifu University), Koji Nishifuji (Tokyo University of Agriculture and Technology), Haruko Ogawa (Obihiro University of Agriculture and Veterinary Medicine), and Masahiro Yamasaki (Iwate University) for giving me valuable ideas and supervising the doctoral study.

I also appreciate all the people in The United Graduate School of Veterinary Sciences and Department of Clinical Veterinary Medicine, Faculty of Applied Biological Sciences, Gifu University for their tremendous help.

Finally, I would like to offer my deepest thanks and appreciation to my wife, Ms. Chinatsu Kanei, for her sincere encouragement, support, and understanding regardless of my reckless challenge.

References

1. Ariyarathna H., Thomson N., Aberdein D., Munday J. S. (2020). Chemokine gene expression influences metastasis and survival time of female dogs with mammary carcinoma. Vet Immunol Immunopathol. 227, 110075.
2. Azuma K., Ohmi A., Goto-Koshino Y., Tomiyasu H., Ohno K., Chambers J. K., Uchida K., Namba H., Nagata M., Nagamine E., Nibe K., Irie M., Tsujimoto H. (2022). Outcomes and prognostic factors in canine epitheliotropic and nonepitheliotropic cutaneous T-cell lymphomas. Vet Comp Oncol. 20 (1). 118-126.
3. Bianchi M. E., Mezzapelle R. (2020). The Chemokine Receptor CXCR4 in Cell Proliferation and Tissue Regeneration. Front Immunol. 11, 2109.
4. Bromley S. K., Mempel T. R., Luster A. D. (2008). Orchestrating the orchestrators: chemokines in control of T cell traffic. Nat Immunol. 9 (9). 970-980.
5. Bromley S. K., Thomas S. Y., Luster A. D. (2005). Chemokine receptor CCR7 guides T cell exit from peripheral tissues and entry into afferent lymphatics. Nat. Immunol. 6 (9). 895-901.
6. Carbonell W. S., Ansorge O., Sibson N., Muschel R. (2009). The vascular basement membrane as "soil" in brain metastasis. PLoS One. 4 (6). e5857.
7. Chan C. M., Frimberger A. E., Moore A. S. (2018). Clinical outcome and prognosis of dogs with histopathological features consistent with epitheliotropic lymphoma: a retrospective study of 148 cases (2003-2015). Vet Dermatol. 29 (2). 154-e159.
8. Chen L., Liu X., Zhang H. Y., Du W., Qin Z., Yao Y., Mao Y., Zhou L. (2014). Upregulation of chemokine receptor CCR10 is essential for glioma proliferation, invasion and patient survival. Oncotarget. 5 (16). 6576-6583.
9. Chimura N., Kondo N., Shibata S., Kimura T., Mori T., Hoshino Y., Murayama N., Nagata M., Ide K., Nishifuji K., Kamishina H., Maeda S. (2011). Gene transcription analysis in lesional skin of canine epitheliotropic cutaneous lymphoma using quantitative real-time RT-PCR. Vet Immunol Immunopathol. 144 (3-4). 329-336.
10. Crowe A. R., Yue W. (2019). Semi-quantitative Determination of Protein Expression using Immunohistochemistry Staining and Analysis: An Integrated Protocol. Bio Protoc. 9 (24).
11. Debes G. F., Arnold C. N., Young A. J., Krautwald S., Lipp M., Hay J. B., Butcher E. C. (2005). Chemokine receptor CCR7 required for T lymphocyte exit from peripheral tissues. Nat Immunol. 6 (9). 889-894.
12. Delfau-Larue M. H., Petrella T., Lahet C., Lebozec C., Bagot M., Roudot-Thoraval F., Dalac S., Farcet J. P., Wechsler J. (1998). Value of clonality studies of cutaneous T lymphocytes in the diagnosis and follow-up of patients with mycosis fungoides. J Pathol. 184 (2). 185-190.
13. Dillekas H., Rogers M. S., Straume O. (2019). Are 90% of deaths from cancer caused

by metastases? Cancer Med. 8 (12). 5574-5576.

14. Fan T. M., Barger A. M., Fredrickson R. L., Fitzsimmons D., Garrett L. D. (2008). Investigating CXCR4 expression in canine appendicular osteosarcoma. J Vet Intern Med. 22 (3). 602-608.
15. Fontaine J., Bovens C., Bettenay S., Mueller R. S. (2009). Canine cutaneous epitheliotropic T-cell lymphoma: a review. Vet Comp Oncol. 7 (1). 1-14.
16. Fontaine J., Heimann M., Day M. J. (2010). Canine cutaneous epitheliotropic T-cell lymphoma: a review of 30 cases. Vet Dermatol. 21 (3). 267-275.
17. Forster R., Schubel A., Breitfeld D., Kremmer E., Renner-Muller I., Wolf E., Lipp M. (1999). CCR7 coordinates the primary immune response by establishing functional microenvironments in secondary lymphoid organs. Cell. 99 (1). 23-33.
18. Foster A. P., Evans E., Kerlin R. L., Vail D. M. (1997). Cutaneous T-cell lymphoma with Sezary syndrome in a dog. Vet Clin Pathol. 26 (4). 188-192.
19. Gadalla R., Hassan H., Ibrahim S. A., Abdullah M. S., Gaballah A., Greve B., El-Deeb S., El-Shinawi M., Mohamed M. M. (2019). Tumor microenvironmental plasmacytoid dendritic cells contribute to breast cancer lymph node metastasis via CXCR4/SDF-1 axis. Breast Cancer Res Treat. 174 (3). 679-691.
20. Ghadjar P., Coupland S. E., Na I. K., Noutsias M., Letsch A., Stroux A., Bauer S., Buhr H. J., Thiel E., Scheibenbogen C., Keilholz U. (2006). Chemokine receptor CCR6 expression level and liver metastases in colorectal cancer. J Clin Oncol. 24 (12). 1910-1916.
21. Goto-Koshino Y., Mochizuki H., Sato M., Nakashima K., Hiyoshi S., Fujiwara-Igarashi A., Maeda S., Nakamura K., Uchida K., Fujino Y., Ohno K., Tsujimoto H. (2015). Construction of a multicolor GeneScan analytical system to detect clonal rearrangements of immunoglobulin and T cell receptor genes in canine lymphoid tumors. Vet Immunol Immunopathol. 165 (1-2). 81-87.
22. Hara K., Iio A., Asahina R., Takahashi M., Mori T., Nishida H., Kamishina H., Sakai H., Kitoh K., Mizuno T., Tsujimoto H., Maeda S. (2017). Characterization of a novel canine T-cell line established from a dog with cutaneous T-cell lymphoma. J Dermatol Sci. 88 (2). 254-256.
23. Hargreaves D. C., Hyman P. L., Lu T. T., Ngo V. N., Bidgol A., Suzuki G., Zou Y. R., Littman D. R., Cyster J. G. (2001). A coordinated change in chemokine responsiveness guides plasma cell movements. J. Exp. Med. 194 (1). 45-56.
24. Hartley A. N., Tarleton R. L. (2015). Chemokine receptor 7 (CCR7)-expression and IFNgamma production define vaccine-specific canine T-cell subsets. Vet. Immunol. Immunopathol. 164 (3-4). 127-136.
25. Hillman L. A., Garrett L. D., de Lorimier L. P., Charney S. C., Borst L. B., Fan T. M.

(2010). Biological behavior of oral and perioral mast cell tumors in dogs: 44 cases (1996-2006). J. Am. Vet. Med. Assoc. 237 (8). 936-942.

26. Huang E. H., Singh B., Cristofanilli M., Gelovani J., Wei C., Vincent L., Cook K. R., Lucci A. (2009). A CXCR4 antagonist CTCE-9908 inhibits primary tumor growth and metastasis of breast cancer. J Surg Res. 155 (2). 231-236.
27. Iio A., Motohashi T., Kunisada T., Yasuhira Y., Kamishina H., Maeda S. (2014). Preferential gene transcription of T helper 2 cytokines in peripheral CCR4(+) CD4(+) lymphocytes in dogs. Vet. Dermatol. 25 (3). 199-e150.
28. Ikeuchi M., Asahina R., Nishida H., Kamishina H., Kitoh K., Sakai H., Maeda S. (2018). Phenotypic analysis of mice xenografted with canine epitheliotropic cutaneous T-cell lymphoma cells. Vet Dermatol. 29 (6). 517-e172.
29. Iyer A., Hennessey D., O'Keefe S., Patterson J., Wang W., Wong G. K., Gniadecki R. (2019). Skin colonization by circulating neoplastic clones in cutaneous T-cell lymphoma. Blood. 134 (18). 1517-1527.
30. Johnson J. A., Patterson J. M. (1981). Canine epidermotropic lymphoproliferative disease resembling pagetoid reticulosis in man. Vet Pathol. 18 (4). 487-493.
31. Kaczmarek E., Gorna A., Majewski P. (2004). Techniques of image analysis for quantitative immunohistochemistry. Rocz Akad Med Bialymst. 49 Suppl 1, 155-158.
32. Kanei T., Iwata M., Kamishina H., Mizuno T., Maeda S. (2022). Expression and functional analysis of chemokine receptor 7 in canine lymphoma cell lines. J Vet Med Sci. 84 (1). 25-30.
33. Karaman S., Detmar M. (2014). Mechanisms of lymphatic metastasis. J Clin Invest. 124 (3). 922-928.
34. Kawada K., Hosogi H., Sonoshita M., Sakashita H., Manabe T., Shimahara Y., Sakai Y., Takabayashi A., Oshima M., Taketo M. M. (2007). Chemokine receptor CXCR3 promotes colon cancer metastasis to lymph nodes. Oncogene. 26 (32). 4679-4688.
35. Keating M. K., Rosenkrantz W. S., Keller S. M., Moore P. F. (2022). Evaluation of clonality from multiple anatomic sites in canine epitheliotropic T cell lymphoma. Vet Dermatol.
36. Keller S. M., Moore P. F. (2012). A novel clonality assay for the assessment of canine T cell proliferations. Vet Immunol Immunopathol. 145 (1-2). 410-419.
37. Keller S. M., Moore P. F. (2012). Rearrangement patterns of the canine TCRgamma locus in a distinct group of T cell lymphomas. Vet Immunol Immunopathol. 145 (1-2). 350-361.
38. Kempf W., Mitteldorf C. (2021). Cutaneous T-cell lymphomas-An update 2021. Hematol Oncol. 39 Suppl 1, 46-51.
39. Kienast Y., von Baumgarten L., Fuhrmann M., Klinkert W. E., Goldbrunner R.,

Herms J., Winkler F. (2010). Real-time imaging reveals the single steps of brain metastasis formation. Nat Med. 16 (1). 116-122.

40. Knecht H., Joske D. J., Bachmann E., Bachmann F., Odermatt B. F., Pallesen G. (1993). Expression of human recombination activating genes (RAG-1 and RAG-2) in angioimmunoblastic lymphadenopathy and anaplastic large cell lymphoma of T-type. Br J Haematol. 83 (4). 655-659.
41. Knoblaugh S. E., Himmel L. E. (2019). Keeping Score: Semiquantitative and Quantitative Scoring Approaches to Genetically Engineered and Xenograft Mouse Models of Cancer. Vet Pathol. 56 (1). 24-32.
42. Kunkel E. J., Butcher E. C. (2002). Chemokines and the tissue-specific migration of lymphocytes. Immunity. 16 (1). 1-4.
43. Labun K., Montague T. G., Krause M., Torres Cleuren Y. N., Tjeldnes H., Valen E. (2019). CHOPCHOP v3: expanding the CRISPR web toolbox beyond genome editing. Nucleic Acids Res. 47 (W1). W171-W174.
44. Li J. Y., Ou Z. L., Yu S. J., Gu X. L., Yang C., Chen A. X., Di G. H., Shen Z. Z., Shao Z. M. (2012). The chemokine receptor CCR4 promotes tumor growth and lung metastasis in breast cancer. Breast Cancer Res Treat. 131 (3). 837-848.
45. Liu L. B., Xie F., Chang K. K., Shang W. Q., Meng Y. H., Yu J. J., Li H., Sun Q., Yuan M. M., Jin L. P., Li D. J., Li M. Q. (2015). Chemokine CCL17 induced by hypoxia promotes the proliferation of cervical cancer cell. Am J Cancer Res. 5 (10). 3072-3084.
46. Lu E., Cyster J. G. (2019). G-protein coupled receptors and ligands that organize humoral immune responses. Immunol Rev. 289 (1). 158-172.
47. Maeda S., Ohno K., Tsukamoto A., Nakashima K., Fukushima K., Goto-Koshino Y., Fujino Y., Tsujimoto H. (2012). Molecular cloning and expression analysis of the canine chemokine receptor CCR9. Vet Immunol Immunopathol. 145 (1-2). 534-539.
48. Maeda S., Okayama T., Omori K., Masuda K., Sakaguchi M., Ohno K., Tsujimoto H. (2002). Expression of CC chemokine receptor 4 (CCR4) mRNA in canine atopic skin lesion. Vet Immunol Immunopathol. 90 (3-4). 145-154.
49. Mashino K., Sadanaga N., Yamaguchi H., Tanaka F., Ohta M., Shibuta K., Inoue H., Mori M. (2002). Expression of chemokine receptor CCR7 is associated with lymph node metastasis of gastric carcinoma. Cancer Res. 62 (10). 2937-2941.
50. Mineshige T., Kawarai S., Yauchi T., Segawa K., Neo S., Sugahara G., Kamiie J., Hisasue M., Shirota K. (2016). Cutaneous epitheliotropic T-cell lymphoma with systemic dissemination in a dog. J Vet Diagn Invest. 28 (3). 327-331.
51. Mo M., Zhou M., Wang L., Qi L., Zhou K., Liu L. F., Chen Z., Zu X. B. (2015). CCL21/CCR7 enhances the proliferation, migration, and invasion of human bladder cancer T24 cells. PLoS One. 10 (3). e0119506.

52. Moore A. S. (2016). Treatment of T cell lymphoma in dogs. Vet Rec. 179 (11). 277.
53. Moore P. F., Olivry T., Naydan D. (1994). Canine cutaneous epitheliotropic lymphoma (mycosis fungoides) is a proliferative disorder of CD8+ T cells. Am J Pathol. 144 (2). 421-429.
54. Moroki T., Matsuo S., Hatakeyama H., Hayashi S., Matsumoto I., Suzuki S., Kotera T., Kumagai K., Ozaki K. (2021). Databases for technical aspects of immunohistochemistry: 2021 update. J Toxicol Pathol. 34 (2). 161-180.
55. Muller A., Homey B., Soto H., Ge N., Catron D., Buchanan M. E., McClanahan T., Murphy E., Yuan W., Wagner S. N., Barrera J. L., Mohar A., Verastegui E., Zlotnik A. (2001). Involvement of chemokine receptors in breast cancer metastasis. Nature. 410 (6824). 50-56.
56. Naito Y., Hino K., Bono H., Ui-Tei K. (2015). CRISPRdirect: software for designing CRISPR/Cas guide RNA with reduced off-target sites. Bioinformatics. 31 (7). 1120-1123.
57. Rapp M., Wintergerst M. W. M., Kunz W. G., Vetter V. K., Knott M. M. L., Lisowski D., Haubner S., Moder S., Thaler R., Eiber S., Meyer B., Rohrle N., Piseddu I., Grassmann S., Layritz P., Kuhnemuth B., Stutte S., Bourquin C., von Andrian U. H., Endres S., Anz D. (2019). CCL22 controls immunity by promoting regulatory T cell communication with dendritic cells in lymph nodes. J Exp Med. 216 (5). 1170-1181.
58. Ren Y., Kan Y. Z., Kong L. F. (2018). Study on the effects of target-silencing CXCR3 expression on malignant proliferation of hepatocellular carcinoma. Zhonghua Gan Zang Bing Za Zhi. 26 (7). 508-512.
59. Richmond A. (2008). CCR9 homes metastatic melanoma cells to the small bowel. Clin Cancer Res. 14 (3). 621-623.
60. Rizeq B., Malki M. I. (2020). The Role of CCL21/CCR7 Chemokine Axis in Breast Cancer Progression. Cancers (Basel). 12 (4).
61. Rizzardi A. E., Johnson A. T., Vogel R. I., Pambuccian S. E., Henriksen J., Skubitz A. P., Metzger G. J., Schmechel S. C. (2012). Quantitative comparison of immunohistochemical staining measured by digital image analysis versus pathologist visual scoring. Diagn Pathol. 7, 42.
62. Rudolphi A., Spiess S., Conradt P., Claesson M. H., Reimann J. (1991). CD3+ T cells in severe combined immune deficiency (scid) mice. I. Transferred purified CD4+ T cells, but not CD8+ T cells are engrafted in the spleen of congenic scid mice. Eur J Immunol. 21 (2). 523-533.
63. Sahai E. (2007). Illuminating the metastatic process. Nat Rev Cancer. 7 (10). 737-749.
64. Sallusto F., Baggiolini M. (2008). Chemokines and leukocyte traffic. Nat. Immunol. 9 (9). 949-952.

65. Schatz D. G., Oettinger M. A., Baltimore D. (1989). The V(D)J recombination activating gene, RAG-1. Cell. 59 (6). 1035-1048.
66. Shadduck J. A., Reedy L., Lawton G., Freeman R. (1978). A canine cutaneous lymphoproliferative disease resembling mycosis fungoides in man. Vet Pathol. 15 (6). 716-724.
67. Sun L., Zhang Q., Li Y., Tang N., Qiu X. (2015). CCL21/CCR7 up-regulate vascular endothelial growth factor-D expression via ERK pathway in human non-small cell lung cancer cells. Int. J. Clin. Exp. Pathol. 8 (12). 15729-15738.
68. Takekoshi T., Fang L., Paragh G., Hwang S. T. (2012). CCR7-expressing B16 melanoma cells downregulate interferon-gamma-mediated inflammation and increase lymphangiogenesis in the tumor microenvironment. Oncogenesis. 1, e9.
69. Tang H. L., Cyster J. G. (1999). Chemokine Up-regulation and activated T cell attraction by maturing dendritic cells. Science. 284 (5415). 819-822.
70. Teijeira A., Hunter M. C., Russo E., Proulx S. T., Frei T., Debes G. F., Coles M., Melero I., Detmar M., Rouzaut A., Halin C. (2017). T Cell Migration from Inflamed Skin to Draining Lymph Nodes Requires Intralymphatic Crawling Supported by ICAM-1/LFA-1 Interactions. Cell Rep. 18 (4). 857-865.
71. Umeki S., Ema Y., Suzuki R., Kubo M., Hayashi T., Okamura Y., Yamazaki J., Tsujimoto H., Tani K., Hiraoka H., Okuda M., Mizuno T. (2013). Establishment of five canine lymphoma cell lines and tumor formation in a xenotransplantation model. J. Vet. Med. Sci. 75 (4). 467-474.
72. Vega F., Luthra R., Medeiros L. J., Dunmire V., Lee S. J., Duvic M., Jones D. (2002). Clonal heterogeneity in mycosis fungoides and its relationship to clinical course. Blood. 100 (9). 3369-3373.
73. Vestergaard C., Bang K., Gesser B., Yoneyama H., Matsushima K., Larsen C. G. (2000). A Th2 chemokine, TARC, produced by keratinocytes may recruit CLA+CCR4+ lymphocytes into lesional atopic dermatitis skin. J Invest Dermatol. 115 (4). 640-646.
74. Vestergaard C., Yoneyama H., Murai M., Nakamura K., Tamaki K., Terashima Y., Imai T., Yoshie O., Irimura T., Mizutani H., Matsushima K. (1999). Overproduction of Th2-specific chemokines in NC/Nga mice exhibiting atopic dermatitis-like lesions. J Clin Invest. 104 (8). 1097-1105.
75. Vulcano M., Albanesi C., Stoppacciaro A., Bagnati R., D'Amico G., Struyf S., Transidico P., Bonecchi R., Del Prete A., Allavena P., Ruco L. P., Chiabrando C., Girolomoni G., Mantovani A., Sozzani S. (2001). Dendritic cells as a major source of macrophage-derived chemokine/CCL22 in vitro and in vivo. Eur J Immunol. 31 (3). 812-822.
76. Willemze R., Cerroni L., Kempf W., Berti E., Facchetti F., Swerdlow S. H., Jaffe E. S.

(2019). The 2018 update of the WHO-EORTC classification for primary cutaneous lymphomas. Blood. 133 (16). 1703-1714.

77. Xu Y., Liu L., Qiu X., Jiang L., Huang B., Li H., Li Z., Luo W., Wang E. (2011). CCL21/CCR7 promotes G2/M phase progression via the ERK pathway in human non-small cell lung cancer cells. PLoS One. 6 (6). e21119.

78. Yagihara H., Tamura K., Isotani M., Ono K., Washizu T., Bonkobara M. (2007). Genomic organization of the T-cell receptor gamma gene and PCR detection of its clonal rearrangement in canine T-cell lymphoma/leukemia. Vet Immunol Immunopathol. 115 (3-4). 375-382.

79. Yang J., Wang S., Zhao G., Sun B. (2011). Effect of chemokine receptors CCR7 on disseminated behavior of human T cell lymphoma: clinical and experimental study. J. Exp. Clin. Cancer. Res. 30, 51.

80. Yarnall B. W., Chamberlain C. S., Hao Z., Muir P. (2019). Proinflammatory polarization of stifle synovial macrophages in dogs with cruciate ligament rupture. Vet. Surg. 48 (6). 1005-1012.

81. Yoneda N., Tatsumi E., Kawano S., Matsuo Y., Minowada J., Yamaguchi N. (1993). Human recombination activating gene-1 in leukemia/lymphoma cells: expression depends on stage of lymphoid differentiation defined by phenotype and genotype. Blood. 82 (1). 207-216.

82. Yoshie O., Matsushima K. (2015). CCR4 and its ligands: from bench to bedside. Int Immunol. 27 (1). 11-20.

83. Yu S., Duan J., Zhou Z., Pang Q., Wuyang J., Liu T., He X., Xinfa L., Chen Y. (2008). A critical role of CCR7 in invasiveness and metastasis of SW620 colon cancer cell in vitro and in vivo. Cancer Biol. Ther. 7 (7). 1037-1043.

84. Zandvliet M. (2016). Canine lymphoma: a review. Vet Q. 36 (2). 76-104.

85. Zhao L., Wang Y., Xue Y., Lv W., Zhang Y., He S. (2015). Critical roles of chemokine receptor CCR5 in regulating glioblastoma proliferation and invasion. Acta Biochim Biophys Sin (Shanghai). 47 (11). 890-898.

86. Zlotnik A., Yoshie O. (2012). The chemokine superfamily revisited. Immunity. 36 (5). 705-716.